Electron Transfer at Metal Surfaces

Thesis by

Shachi S. Gosavi

In Partial Fulfillment of the Requirements

for the Degree of

Doctor of Philosophy

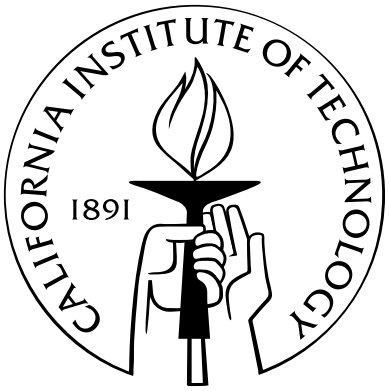

California Institute of Technology

Pasadena, California

2002

(Submitted Aug 9, 2002)

Acknowledgements

I thank my advisor, Prof. Marcus, for his guidance and support throughout my thesis work. I thank my committee members for their patience and insightful comments during the various examinations. I would like to thank Prof. Finklea, Prof. Forster and Prof. Lewis for bringing to our attention interesting experimental results and problems.

Finally, I thank various past and present members of the Marcus group, Ruth DeSilveira, Billie Tone, and Tom Dunn for teaching, supporting, and helping me and making my stay at Caltech a pleasant and comfortable one.

Thesis Abstract

In recent years, there has been much interest in electrode processes at metal surfaces with monolayers coated on them. These monolayers are typically composed of alkanethiol molecules. The advantage of alkanethiol molecules is that their length can be changed systematically. The electron transfer rate across an alkanethiol interface can be measured as a function of the length of the alkanethiol chain length. A method using Green's functions was developed in our laboratory to treat the electron transfer rate across a monolayer covered electrode.

Another effect of the monolayer is that the electron transfer rate from the redox reagent in solution to the metal (gold or platinum is commonly used) becomes clearly nonadiabatic in nature. Thus, the effect of the density of states of the metal on such a rate can be investigated. We used the previously developed method of Green's functions to calculate the change in the electron transfer rate constant on changing the metal electrode. We developed a way of writing the wave function of a semi-infinite metal using tight-binding matrix elements and the Z-transform. Using these **k** dependent metal wave functions we could calculate the coupling matrix element between the metal and the redox reagent and thus calculate the electron transfer rate constant k_{ET}.

We used this method to study the effect of changing the density of electronic states, ρ_{F}, at the Fermi level of a metal on the rate of nonadiabatic electron transfer. The rate constant k_{ET} was calculated for the electron transfer to platinum and to gold using the equation

$$k_{ET} = \frac{2\pi}{\hbar} \int d\epsilon \left[\frac{e^{-(\lambda - e\eta + \epsilon)^2 / 4\lambda k_B T}}{(4\pi\lambda k_B T)^{1/2}} \right] |V(\epsilon)|^2 f(\epsilon), \tag{1}$$

where λ is the reorganization energy, e is the electronic charge, and η is the overpotential. The expression in [ ] is the classical Franck-Condon factor. $V(\epsilon)$ is the coupling matrix element calculated by the method of Green's functions and the Z-transform. $f(\epsilon)$ is the Fermi-Dirac distribution function.

The ρ_{F} of platinum is about 7.5 times that of gold, the difference being mainly due to the *d*-band of Pt. In spite of this difference, the calculated electron transfer rate constant k_{ET} increases only by a factor of about 1.8, instead of the factor of about 7.5 expected using ρ_{F} alone. Bands which are weakly coupled (*e.g.*, the *d*-band of Pt in the present case) contribute much less to the rate constant than is suggested by their density of states ρ_{F}. Thereby, k_{ET} is approximately independent of ρ_{F} in two cases: adiabatic electron transfer and nonadiabatic electron transfer when the extra ρ_{F} is due to the *d*-electrons. Our results are in agreement with experiments performed with systems similar to those used in our calculations.

We then employed our method to calculate the temperature dependence of the electronic contribution to the nonadiabatic electron transfer rate constant (k_{ET}) at metal electrodes. It was found in our calculations that this contribution is proportional to the absolute temperature T. The Fermi function and the Franck-Condon factor broaden with temperature. This broadening implies that a broader distribution of metal electronic states about the Fermi level is sampled with increasing T. The electronic contribution is linear in T because the density of states is approximately constant with energy, narrow, quickly varying bands contributing less to the coupling matrix element than broader $s-p$ type bands as before.

We also considered the nonadiabatic rate constant for electron transfer at a semiconductor electrode. Under conditions for the maximum rate constant, the electronic contribution is also estimated to be proportional to T, but for different reasons than in the case of metals (Boltzmann statistics and transfer at the conduction band edge for the semiconductor *vs.* Fermi-Dirac statistics and transfer at the Fermi level, which is far from the band edge, of the metal).

On a different topic, we study the inverse photoemission spectra at metal electrodes. Inverse photoemission at the solid-vacuum interface can be used to map the empty electronic states above the Fermi level of the metal. Several years ago, experiments were performed at the metal-solution interface similar in nature to inverse photoemission spectroscopy. In these experiments, an electron transfer redox agent was used to inject electons or holes into a metal and create excited states. These

excited states decayed radiatively to give a frequency dependent spectrum. This spectrum may be analysed to map the electronic structure of the metal above and below its Fermi level. This experimental technique is known as charge transfer inverse photoemission spectroscopy (CTRIPS).

We make a compilation of all the available CTRIPS data, and list the principal features of the spectra. We also bring out some inconsistencies in the data which need clarification. We present a simple model of the electron transfer process and the emission. We give some possible explanations of the data using our model, experimental band structures (from vacuum inverse photemission) and solution electroreflectance (ER) experiments. We also propose some experiments that could be performed to further clarify the electronic structure of the metal in solution.

Contents

List of Figures

List of Tables

Chapter 1

Introduction

Electron transfer (ET) from a solvated donor to a solvated acceptor or between a solvated donor/acceptor and an electrode is among the simplest of the chemical reactions, there being no bond formation or bond breaking involved. In this thesis, we study the latter and discuss ET processes at metal-solution interfaces. Electron transfer processes [eq 1.1],

$$D + A \longrightarrow D^+ + A^-, \tag{1.1}$$

are usually represented in terms of Marcus parabolas [Fig. 1.1]. These parabolas are the free energy curves for the reactant state (D, A, solution) and the product state (D^+, A^-, solution). The statistical mechanical analysis is based on multi-dimensional (thousands of coordinates) potential energy surfaces and the definition of a suitable reaction coordinate, Q. A statistical mechanical calculation at each Q yields the free energy parabolas. The electron being a light particle, the reaction follows the Franck-Condon principle, and the donor, acceptor, and solvent molecules are assumed to be stationary during the electron tunnelling event. The transfer also satisfies energy conservation. Thus, for a dark transition the system moves from the reactants' parabola to the products' parabola only at their intersection.

The reactants travel along the reactant parabola up to and beyond the point of intersection, $Q^\ddagger$. At $Q^\ddagger$ there is a possibility of electron transfer through electron tunnelling from the reactant state to the product state. The ET rate constant can

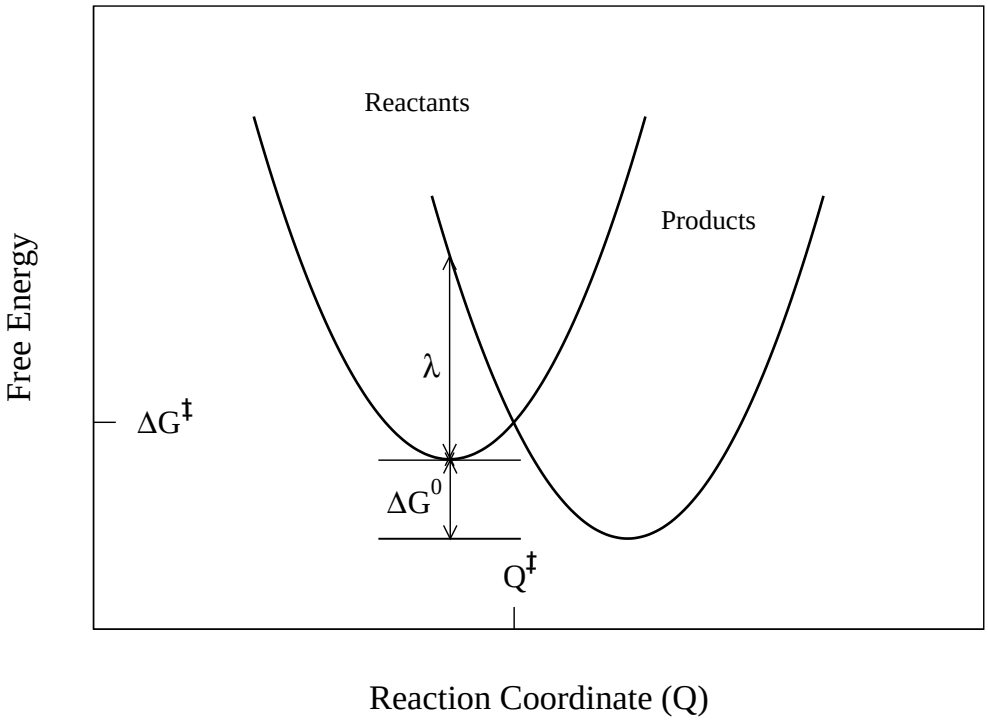

Figure 1.1: Free energy of the ET reaction.

be modelled as

$$\begin{aligned} k_{ET} &= P(\text{Reactant diffusion to reach intersection of parabolas}) \\ &\times P(\text{Electron tunnelling}), \end{aligned} \tag{1.2}$$

where P(event) is the probability of the 'event' happening. The first part of the RHS of eq 1.2 is due to solvent relaxation and the temperature of the system, while the second is due to the electronic coupling matrix element between the reactant and the product states. This matrix element facilitates the electron transfer.

On the basis of eq 1.2, ET processes are usually classified into two types:

1. **Adiabatic:** When the average time for a tunnelling event is small compared to the time the system spends near $Q^{\ddagger}$ (in reaction coordinate space) the electron tunnelling event occurs almost every time the electron reaches $Q^{\ddagger}$ or P(Electron tunnelling) ≈ 1. The simplest case for which this condition applies is that of a reacting system with a large electronic coupling matrix element between donor and acceptor. Using the approximation, the rate constant can be written as

$$\begin{aligned} k_{ET} &= P(\text{Reactant diffusion to reach intersection of parabolas}) \\ &= A\, e^{-\Delta G^{\ddagger}/k_B T}, \end{aligned} \tag{1.3}$$

   which is just the Arrehenius probability of reaching $Q^{\ddagger}$ from the bottom of the reactants' parabola. Using the parabolic model $\Delta G^{\ddagger}$ can be evaluated:

$$\Delta G^{\ddagger} = \frac{(\Delta G^0 + \lambda)^2}{4\lambda}, \tag{1.4}$$

   where λ, the reorganization energy, is the energy required to change the configuration of the reactants into the equilibrium configuration of the products without the electron transfer having taken place.

   Examples of systems in which adiabatic electron transfer occurs are small sol-

vated molecules [1].

2. **Nonadiabatic:** When the tunnelling matrix element is small, the system has to diffuse up to $Q^{\ddagger}$ (in reaction coordinate space) several times before the electron tunnels. Such a weak coupling case can be treated quantum mechanically using the Fermi's golden rule. In the nonadiabatic case k_{ET} can be written as

$$k_{ET} = \frac{2\pi}{\hbar}|H_{DA}|^2 FC, \tag{1.5}$$

where H_{DA} is the electronic coupling matrix element between the donor and the acceptor. FC is the Franck-Condon factor and is equal to $\frac{\exp(-(\Delta G^0+\lambda)^2/4\lambda k_B T)}{(4\pi\lambda k_B T)^{1/2}}$ in the classical case.

Nonadiabatic electron transfer usually occurs over long distances and has been studied extensively both in bridged systems in solution [2] and across monolayers on electrodes [3].

In the present thesis, we study nonadiabatic electron transfer at metal-solution interfaces.

1.1 Electron transfer at metal surfaces

Metals have a continuum of donor/acceptor states. Each of these states has to be included in the ET calculation. Whether ET at the metal-solution interface is adiabatic or nonadiabatic depends on the distance between the electrode and the redox agent in solution. It thus depends on the structure of the metal-solution interface.

In recent years there has been a lot of interest in electrode processes at metal surfaces with monolayers coated on them. An effect of the monolayer is that the electron transfer rate from the redox reagent in solution to the metal (gold or platinum is commonly used) becomes clearly nonadiabatic in nature.

The monolayers are typically composed of alkanethiol molecules. The advantage of alkanethiol molecules is that their length can be changed systematically. The

electron transfer rate across an alkanethiol interface can be measured as a function of the length of the alkanethiol chain length. A method using Green's functions was developed in our laboratory to treat the electron transfer rate across a monolayer covered electrode.

In the present thesis, we investigate the effect of changing the density of electronic states, ρ_{F}, at the Fermi level of a metal on the rate of nonadiabatic electron transfer. We use the previously developed method of Green's functions to calculate the change in the electron transfer rate constant on changing the metal electrode. We develop a method for writing the wave function of a semi-infinite metal using tight-binding matrix elements and the Z-transform. Using these **k**-dependent metal wave functions, we calculate the coupling matrix element between the metal and the redox reagent and thus calculate the electron transfer rate constant k_{ET}.

Au(111) and Pt(111) are ideal systems for our study, the ρ_{F} of Pt is about 7.5 times that of Au, the difference being mainly due to the *d*-band of Pt. In spite of this difference, experiments have found that the electron transfer rate constant k_{ET} increases only by a factor of about 1.7, instead of the factor of about 7.5 expected using ρ_{F} alone. We find that bands which are weakly coupled (e.g., the *d*-band of Pt in the present case) contribute much less to the rate constant than is suggested by their ρ_{F}. Thereby, k_{ET} is approximately independent of ρ_{F} in two cases: adiabatic electron transfer and nonadiabatic electron transfer when the extra ρ_{F} is due to weakly coupled bands such as *d*-electrons. There is good agreement between calculated and experimentally observed ratios k_{ET}^{Pt}/k_{ET}^{Au}.

We also employ our method to calculate the temperature dependence of the electronic contribution to the nonadiabatic electron transfer rate constant (k_{ET}) at metal electrodes. We find that this contribution is proportional to the absolute temperature T. We also consider the nonadiabatic rate constant for electron transfer at a semiconductor electrode. Under conditions for the maximum rate constant, this electronic contribution is also estimated to be proportional to T, but for different reasons than in the case of metals (Boltzmann statistics and transfer at the conduction band edge for the semiconductor *vs.* Fermi-Dirac statistics and transfer at the Fermi level, which

is far from the band edge, for the metal).

1.2 Photoemission at metal surfaces

On a different topic, we study the inverse photoemission spectra at metal electrodes. Inverse photoemission at the solid-vacuum interface can be used to map the empty electronic states above the Fermi level of the metal. Several years ago, experiments were performed at the metal-solution interface similar in nature to inverse photoemission spectroscopy in vacuum. In these experiments, an electron transfer redox agent was used to inject electons or holes into a metal and create excited states. These excited states decayed radiatively to give a frequency dependent spectrum. This spectrum may be analysed to map the electronic structure of the metal above and below its Fermi level. This experimental technique is known as charge transfer inverse photoemission spectroscopy (CTRIPS). We make a compilation of all the available CTRIPS data, and list the principal features of the spectra. We also bring out some inconsistencies in the data which need clarification. We present a simple model for the electron transfer process and the emission of light. We give a possible explanation of the data using our model, experimental band structures (from vacuum inverse photemission) and solution electroreflectance (ER) experiments, which accounts for the principal experimental results. We also propose some experiments that could be performed to further clarify the electronic structure of the metal in solution.

The next three chapters are self-contained. A formulation for calculating wave functions using the Z-transform and the results on changing the density of states at metal surfaces are given in Chapter 2. Results on the temperature dependence of the electronic factor in nonadiabatic ET at metal and semiconductor electrodes are presented in Chapter 3. The study on inverse photoemission at a metal-solution interface is presented in Chapter 4. The conclusions are summarized in Chapter 5.

Chapter 2

Nonadiabatic Electron Transfer at Metal Surfaces

2.1 Introduction

In this chapter, we study how the rate of electron transfer is affected by the density (ρ_{F}) and the nature of electronic states of the metal at the Fermi level, in particular how the exchange current, is affected. There have been some experiments performed investigating the variation of the rate constant with the density of states of the metal not using monolayers [4, 5, 6] and with monolayers [7, 8]. Iwasita *et al.* [4] measured the electrochemical exchange current i_{ex} for the $\mathrm{Ru(NH_3)_6^{2+} - Ru(NH_3)_6^{3+}}$ couple at several metal electrodes. They found that i_{ex} was the same, even when the density of electronic states differed by an order of magnitude.

The first explanation that comes to mind for such experiments [4, 5, 6] is that the electron transfer reaction is adiabatic. The exchange current, i_{ex}, is expected to be proportional to ρ_{F} only for nonadiabatic electron transfers, namely, in the limit of weak coupling of the redox agent to the metal. In the adiabatic case, i_{ex} should be independent of ρ_{F}. However, there is an alternative explanation for the results. The assumption that i_{ex} is proportional to ρ_{F} in a nonadiabatic process is based on the assumption that the different electronic orbitals in the metal, *s, p, d,* which contribute to ρ_{F}, contribute equally to i_{ex}. The large value of ρ_{F} in metals such as Pt or Pd arises because their d orbitals lie near the Fermi level. If the d electrons are much less coupled to the acceptor than the s electrons (which dominate ρ_{F} for metals such

as Au or Ag), the exchange rate would not be proportional to the total ρ_{F} even for a nonadiabatic process.

In recent years, there has been much experimental work with monolayers coated on metal surfaces [9, 10] (mainly gold). Such experiments have been used to study features such as the distance dependence of the rate of electron transfer, the reorganization energy and the coupling between the redox agent and the metal. When a sufficiently thick monolayer is present, for example, sufficiently long alkyl chains in the case of a thioalkane monolayer, the coupling between the metal and the acceptor is weak and the rate of electron transfer is clearly nonadiabatic. Studies with such a system would help differentiate between the two explanations for the rate constant dependence on the density of states given above, by providing information on the coupling by d versus s electrons.

In this chapter, the electron transfer rate constant k_{ET} is calculated for an alkanethiol with 15 methylene units, with the redox agent $\mathrm{Ru(NH_3)_5Py^{2+}}$ tethered to it. A monolayer of the alkanethiol ($\mathrm{HS(CH_2)_{15}CONHCH_2PyRu(NH_3)_5^{2+}}$) is then coated on the (111) face of a metal. We estimate how changing the metal from Pt to Au changes the rate constant and hence the exchange current.

The theoretical model is described in Section 2.2. To treat the metal electrode, a tight-binding (TB) approach is used in the calculations. Parameters available from a fit to band structure of the metals [11] are used. The extended Hückel method [12] is used to treat the alkanethiol bridge and its coupling to the acceptor and to the metal. The bridge part is parametrized to fit experimental band structure of long chain alkanes. In a recent article [13], it was found that this parametrization was sufficiently accurate for the calculation of the distance dependence of long-range electron transfer rates in similar systems.

In treating the metal, the Z-transform [20] method is used, which facilitates the use of a semi-infinite model for the electrode and allows for easy calculation of metal wave functions with tight-binding parameters. This method is summarized in Section 2.4 and is applied there to the present problem. In the present chapter, we use it to explore how k_{ET} changes with a change in ρ_{F}, namely, how it changes with the metal

electrode, and examine particularly the relative contributions of d and s electronic states to the rate constant. The results are discussed in Section 2.5 and compared with available experimental data. The present approach, like that in our earlier papers [15, 16] on long-range electron transfer, is a pragmatic one, namely to use an approximate but simple method which has no arbitrarily adjustable parameters and see whether it is in agreement with the trends in the available experimental results.

2.2 Theoretical model

The standard expression for the first-order rate constant for a nonadiabatic electron transfer (weak electronic coupling limit) for reactants fixed in position is [17]

$$k_{ET} = \frac{2\pi}{\hbar} FC |H_{DA}|^2, \tag{2.1}$$

where FC is the Franck-Condon factor and H_{DA} is the electronic coupling between the donor and the acceptor.

We consider a donor (or acceptor) attached to the electrode by a thioalkane bridge monolayer. When a continuum of donor or acceptor levels is involved in the electron transfer, as is the case in a metal electrode, the right-hand side of eq 2.1 is integrated appropriately over these levels. The rate constant for electron transfer can then be written as [17, 18]

$$k_{ET} = \frac{2\pi}{\hbar} \int d\epsilon \frac{e^{-(\lambda - e\eta + \epsilon)^2/4\lambda k_B T}}{(4\pi\lambda k_B T)^{1/2}} |V(\epsilon)|^2 f(\epsilon) \tag{2.2}$$

and the units of k_{ET} are s^{-1}. For the Franck-Condon factor we have substituted a classical value (the final ratio k_{ET}'s for different metals will be insensitive to this approximation),

$$FC = \frac{e^{-(\lambda - e\eta + \epsilon)^2/4\lambda k_B T}}{(4\pi\lambda k_B T)^{1/2}}, \tag{2.3}$$

where λ is the reorganization energy, e is the electronic charge, and η is the overpotential. In eq 2.2, $f(\epsilon)$ is the Fermi-Dirac distribution with ϵ measured relative to μ,

the chemical potential of the electrode,

$$f(\epsilon) = \frac{e^{\epsilon/k_BT}}{1 + e^{\epsilon/k_BT}}. \tag{2.4}$$

The square of the coupling matrix element, $|V(\epsilon)|^2$ denotes an integral over all the wavevectors $\mathbf{k}$ which contribute to a given energy,

$$|V(\epsilon)|^2 = \int d^3\mathbf{k}|H_{kA}|^2\delta(\epsilon(\mathbf{k}) - \epsilon). \tag{2.5}$$

$|H_{kA}|$ is $\langle\Psi_\mathrm{k}|H|\Psi_\mathrm{A}\rangle$ and describes the electronic coupling between the redox agent (A) and a particular electronic state of wavevector $\mathbf{k}$ of the electrode (which may have contributions from many bands). The integral over wavevectors in eq 2.5 is intended to include all such states and bands. Ψ_k and Ψ_A are the wave functions of the electrode and the redox agent respectively. Ψ_A is normalized in the usual way and has units of $\mathrm{\AA}^{-3/2}$. For Ψ_k a box normalization is used, i.e.,

$$\frac{\langle\Psi_\mathrm{k}(\mathbf{r})|\Psi_\mathrm{k}(\mathbf{r})\rangle}{\mathrm{V}} = 1, \tag{2.6}$$

where V is the unit cell volume and $\langle\ \rangle$ implies integration over a unit cell volume. Thus, $\Psi_\mathrm{k}(\mathbf{r})$ has no units and $\langle\Psi_\mathrm{k}|H|\Psi_\mathrm{A}\rangle$ acquires units of eV $\mathrm{\AA}^{3/2}$, $|H_{kA}|^2$ has units of eV^2 $\mathrm{\AA}^3$ ($\mathrm{eV}^2\mathrm{wavevector}^{-3}$), and so $|V(\epsilon)|^2$ has units of eV.

The exchange current can be obtained from the rate constant with η set to 0 and then integrating over a unit area of the metal surface. Equation 2.2 is readily modified when the redox reagent is not attached to the monolayer.

For a single-band case, $\eta = 0$ and $\lambda >> \epsilon$ (as is typically the case), eq 2.2 simplifies to [13]

$$k_{ET} = \frac{2\pi}{\hbar}(4\pi\lambda k_BT)^{-1/2}e^{-\lambda/4k_BT}\overline{|V|^2}, \tag{2.7}$$

where

$$\overline{|V|^2} = \pi k_BT\overline{|H_{kA}|^2}\rho_F, \tag{2.8}$$

the square of the coupling $\overline{|H_{kA}|^2}$ denotes

$$\overline{|H_{kA}|^2} = \frac{\int d^3k \ |H_{kA}|^2 \ \delta(\epsilon(\mathbf{k}) - \epsilon_{\mathrm{F}})}{\int d^3k \ \delta(\epsilon(\mathbf{k}) - \epsilon_{\mathrm{F}})}, \tag{2.9}$$

and ρ_F is the density of states [19] at the Fermi level,

$$\rho_{\mathrm{F}} = \int d^3k \ \delta(\epsilon(\mathbf{k}) - \epsilon_{\mathrm{F}}). \tag{2.10}$$

We use the volume of the unit cell (with a one-atom basis when appropriate as in the present case) as the unit volume and the units of ρ_{F} become $\mathrm{eV}^{-1}\mathrm{atom}^{-1}$.

In a multiband case, more than one band contributes to the density of states. If the summation over different bands is included in $\overline{|H_{kA}|^2}$ and ρ_F includes densities from all bands, eq 2.7 is still applicable. $\overline{|H_{kA}|^2}$ has contributions from all bands and depends on how the states are distributed over the bands and how each band couples to the acceptor. Because of this feature, $\overline{|H_{kA}|^2}$ can vary from metal to metal, and so the rate constant is not merely proportional to ρ_F, although eqs 2.7 to 2.9 remain valid. Clearly, the electronic states of bands weakly coupled to the redox agent will not contribute as much to the rate constant as those from bands strongly coupled to it.

To obtain k_{ET} (eqs 2.7 to 2.9), a calculation of H_{kA} at the Fermi energy (ϵ_{F}) is needed. A Green's function method due to Hsu and Marcus [13] is used to obtain the H_{kA}. Some details on their sequential formula, including the key recursion equations used to obtain the matrix elements, are given in the next section. This matrix element is the coupling between the metal $\langle\Psi_{\mathrm{k}}|$ and the acceptor $|\Psi_{\mathrm{A}}\rangle$ states. To find the form of the $\langle\Psi_{\mathrm{k}}|$ states of the metal we use the Z-transform method. This method is outlined in Section 2.4.

2.3 The Sequential formula

In this section we outline the derivation of the sequential formula of Hsu and Marcus [13] and give the key recursion relations which are used in the calculation of H_{kA}.

Consider a bridge consisting of n identical units (in the present case of an alkanethiol monolayer the unit would be $-CH_2-$) each having m molecular orbitals. Let $\mathbf{e}$ be an $m \times m$ diagonal matrix which represents the Hamiltonian of the bridge unit in a basis which diagonalizes it, i.e.,

$$\mathbf{e} = \begin{pmatrix} \varepsilon_1 & 0 & \cdots & 0 \\ 0 & \varepsilon_2 & \cdots & 0 \\ \vdots & \vdots & \ddots & \vdots \\ 0 & 0 & \cdots & \varepsilon_m \end{pmatrix}. \tag{2.11}$$

Let $\mathbf{v}$ be the coupling between the bridge units in the same basis and $\mathbf{v}^T$ be its transpose. Both $\mathbf{v}$ and $\mathbf{v}^T$ are $m \times m$ matrices. With these definitions and the tight-binding assumption, the Hamiltonian of the total bridge becomes

$$H^{(n)} = \left(\begin{array}{ccccc|c} \mathbf{e} & \mathbf{v} & \mathbf{0} & \mathbf{0} & \cdots & \mathbf{0} \\ \mathbf{v}^T & \mathbf{e} & \mathbf{v} & \mathbf{0} & \cdots & \vdots \\ \mathbf{0} & \mathbf{v}^T & \mathbf{e} & \mathbf{v} & \cdots & \vdots \\ \vdots & \vdots & \vdots & \vdots & \ddots & \mathbf{v} \\ \hline \mathbf{0} & \cdots & \cdots & \mathbf{0} & \mathbf{v}^T & \mathbf{e} \end{array}\right). \tag{2.12}$$

The partitions in the above equation splits $H^{(n)}$ into two parts $\mathcal{H}_0^{(n)}$ and $\mathcal{H}_1^{(n)}$, where

$$\mathcal{H}_0^{(n)} = \left(\begin{array}{ccccc|c} \mathbf{e} & \mathbf{v} & \mathbf{0} & \mathbf{0} & \cdots & \mathbf{0} \\ \mathbf{v}^T & \mathbf{e} & \mathbf{v} & \mathbf{0} & \cdots & \vdots \\ \mathbf{0} & \mathbf{v}^T & \mathbf{e} & \mathbf{v} & \cdots & \vdots \\ \vdots & \vdots & \vdots & \vdots & \ddots & \mathbf{0} \\ \hline \mathbf{0} & \cdots & \cdots & \mathbf{0} & \mathbf{0} & \mathbf{e} \end{array}\right) \equiv \left(\begin{array}{c|c} H^{(n-1)} & \mathbf{0} \\ \hline \mathbf{0} & \mathbf{e} \end{array}\right), \tag{2.13}$$

and

$$\mathcal{H}_1^{(n)} = \left(\begin{array}{ccccc|c} \mathbf{0} & \mathbf{0} & \mathbf{0} & \mathbf{0} & \cdots & \mathbf{0} \\ \mathbf{0} & \mathbf{0} & \mathbf{0} & \mathbf{0} & \cdots & \mathbf{0} \\ \mathbf{0} & \mathbf{0} & \mathbf{0} & \mathbf{0} & \cdots & \mathbf{0} \\ \vdots & \vdots & \vdots & \vdots & \ddots & \mathbf{v} \\ \hline \mathbf{0} & \cdots & \cdots & \mathbf{0} & \mathbf{v}^T & \mathbf{0} \end{array}\right), \tag{2.14}$$

so that $H^{(n)} = \mathcal{H}_0^{(n)} + \mathcal{H}_1^{(n)}$. $\mathcal{H}_0^{(n)}$ is the Hamiltonian of a bridge with $(n-1)$ coupled units and 1 uncoupled unit while $\mathcal{H}_1^{(n)}$ is the coupling between the $(n-1)^{\text{st}}$ unit and the n^{th} unit.

Treating $\mathcal{H}_1^{(n)}$ as a perturbation to $\mathcal{H}_0^{(n)}$, the Green's function for $H^{(n)}$ can be rewritten exactly as

$$\begin{aligned} G^{(n)} &= (E\mathbf{1} - H^{(n)})^{-1} = (E\mathbf{1} - \mathcal{H}_0^{(n)} - \mathcal{H}_1^{(n)})^{-1} \\ &= \mathcal{G}_0^{(n)}(\mathbf{1} - \mathcal{H}_1^{(n)}\mathcal{G}_0^{(n)})^{-1}, \end{aligned} \tag{2.15}$$

where $\mathcal{G}_0^{(n)}$ is the Green's function corresponding to $\mathcal{H}_0^{(n)}$, namely,

$$\mathcal{G}_0^{(n)} = (E\mathbf{1} - \mathcal{H}_0^{(n)})^{-1} = \left(\begin{array}{c|c} G^{(n-1)} & \mathbf{0} \\ \hline \mathbf{0} & \Delta^{-1} \end{array}\right), \tag{2.16}$$

and Δ is the $m \times m$ matrix,

$$\Delta = E\mathbf{1} - \mathbf{e}, \tag{2.17}$$

where E is the energy of the electron.

The tight-binding model is used in this formulation, and so only that block of the Green's function which relates to the transition of the electron from the 1^{st} unit to the n^{th} is needed to calculate H_{kA}. This $m \times m$ block is $G_{(1,n)}^{(n)}$. After some manipulation of eq 2.15 a recursion relation for $G_{(1,n)}^{(n)}$ can be obtained,

$$G_{(1,n)}^{(n)} = G_{(1,n-1)}^{(n-1)}\mathbf{v}\Delta^{-1}(\mathbf{1} - \mathbf{v}^T G_{(n-1,n-1)}^{(n-1)}\mathbf{v}\Delta^{-1})^{-1}, \tag{2.18}$$

and

$$G^{(n)}_{(n,n)} = \Delta^{-1}(\mathbf{1} - \mathbf{v}^T G^{(n-1)}_{(n-1,n-1)}\mathbf{v}\Delta^{-1})^{-1}. \tag{2.19}$$

$G^{(n)}_{(n,n)}$ is the $(n,n)^{\text{th}}$ block of $G^{(n)}$. The initial condition of the recursion, namely, $G^{(2)}_{(1,2)}$ and $G^{(2)}_{(2,2)}$ can be obtained by directly solving eq 2.15 as a $2m \times 2m$ matrix equation.

From $G^{(n)}_{(1,n)}$, H_{kA} can be obtained using an equation derived in ref [13]:

$$H_{kA} = V_{k,1} G^{(n)}_{(1,n)} V_{n,A}, \tag{2.20}$$

where $V_{k,1}$ is the coupling of the metal k-states to the bridge and $V_{n,A}$ is the coupling of the bridge to the acceptor.

2.4 The Z-transform model for semi-infinite metals

The Z-transform is a generalization of the discrete Fourier transform and is commonly used in the field of signal processing [20]. The periodicity of crystals makes them very similar to discrete signals and so, the Z-transform can be applied very easily to crystalline solids to obtain their wave functions. It is especially useful in the application of the tight-binding approximation [14].

We consider a crystal as being built up of planes with two-dimensional translational symmetry. Let $\hat{\mathbf{R}}_{\parallel,1}$ and $\hat{\mathbf{R}}_{\parallel,2}$ be the unit vectors which lie in the plane. Henceforth, we denote any vector [21] lying in the plane by

$$\mathbf{R}_{\parallel} = n_1 \hat{\mathbf{R}}_{\parallel,1} + n_2 \hat{\mathbf{R}}_{\parallel,2} \qquad \text{(with integer } n_1 \text{ and } n_2\text{)}. \tag{2.21}$$

When we sum over $R_{\parallel}$ we imply a double sum over n_1 and n_2. $\mathbf{k}_{\parallel}$ in the subsequent notation denotes a wavevector conjugate to $\mathbf{R}_{\parallel}$.

Let $\hat{\mathbf{R}}_{\text{p}}$ be the third unit vector for the unit cell, directed from one of the above

planes to the next. With this notation each plane has a wave function of the form

$$\Phi_j(\mathbf{r}-\mathbf{R}_\mathrm{p}) = \sum_{R_\parallel=-\infty}^{+\infty} \exp(i\mathbf{k}_\parallel \cdot \mathbf{R}_\parallel)\ \Theta_j(\mathbf{r}-\mathbf{R}_\mathrm{p}-\mathbf{R}_\parallel), \tag{2.22}$$

with

$$\mathbf{R}_\mathrm{p} = n\hat{\mathbf{R}}_\mathrm{p}, \tag{2.23}$$

where j is an index which labels the orbitals for each atom and $\Theta_j(\mathbf{r}\ -\mathbf{R}_\mathrm{p}\ -\mathbf{R}_\parallel)$ denotes the orbital centered at $\mathbf{r}\ =\mathbf{R}_\mathrm{p}+\mathbf{R}_\parallel$. The crystals of both Au and Pt have a one-atom basis (one atom in the unit cell) and so we use that basis here, but this method is easily generalized to a larger basis.

The wave function of the crystal is

$$\Psi_\mathrm{k}(\mathbf{r}) = \sum_{n,j} \Phi_j(\mathbf{r}-n\hat{\mathbf{R}}_\mathrm{p})c_{n,j}, \tag{2.24}$$

where $c_{n,j}$ is a factor which we will find using the Z-transform. j is summed over the number of orbitals per unit cell, here numbered 1 to J. n is summed over as many layers as the problem requires, for example, $-\infty$ to $+\infty$ for a bulk crystal, 1 to $+\infty$ for a bulk crystal with a surface, and 1 to a finite m for a slab. The range of n imposes boundary conditions on the wave function, and we will examine later how these conditions affect the wave function. For now, we take n to be a problem-dependent quantity.

Using the Schroedinger equation, multiplying by a particular $\Phi_l(\mathbf{r}-n'\hat{\mathbf{R}}_\mathrm{p})$ and integrating over $\mathbf{r}$, we obtain

$$\langle\Phi_l(\mathbf{r}-n'\hat{\mathbf{R}}_\mathrm{p}) \mid H \mid \Psi_\mathrm{k}\rangle = \epsilon\langle\Phi_l(\mathbf{r}-n'\hat{\mathbf{R}}_\mathrm{p}) \mid \Psi_\mathrm{k}\rangle. \tag{2.25}$$

For the present problem, where the rate constant is being evaluated at the Fermi level (in the "normal region" for rate constants), ϵ equals ϵ_F and from eqs 2.22 to 2.25 we

have

$$\sum_{n,j}\{\langle\Phi_l(\mathbf{r}-n^{'}\hat{\mathbf{R}}_{\rm p})\mid H\mid\Phi_j(\mathbf{r}-n\hat{\mathbf{R}}_{\rm p})\rangle-\epsilon_{\rm F}\langle\Phi_l(\mathbf{r}-n^{'}\hat{\mathbf{R}}_{\rm p})\mid\Phi_j(\mathbf{r}-n\hat{\mathbf{R}}_{\rm p})\rangle\}c_{n,j}=0. \quad (2.26)$$

The above equation can be written in matrix form,

$$\sum_n \mathbf{M}(n^{'}\hat{\mathbf{R}}_{\rm p},n\hat{\mathbf{R}}_{\rm p})\mathbf{c}_n=0, \quad (2.27)$$

where $\mathbf{M}$ is a $J\times J$ matrix (J is the number of orbitals per atom) and $\mathbf{c}_n$ becomes a column vector with J components, its j^{th} component being $c_{n,j}$. Using the tight-binding (TB) approximation, we assume that any given plane interacts within itself,

$$\mathbf{M}(n\hat{\mathbf{R}}_{\rm p},n\hat{\mathbf{R}}_{\rm p})=\mathbf{A}, \quad (2.28)$$

and with its nearest neighbors,

$$\mathbf{M}(n\hat{\mathbf{R}}_{\rm p},(n-1)\hat{\mathbf{R}}_{\rm p}))=\mathbf{B}^{\dagger}, \quad (2.29)$$

$$\mathbf{M}(n\hat{\mathbf{R}}_{\rm p},(n+1)\hat{\mathbf{R}}_{\rm p}))=\mathbf{B}. \quad (2.30)$$

$\mathbf{A}$, $\mathbf{B}$ and $\mathbf{B}^{\dagger}$ are $J\times J$ matrices (with J same as above) which can be calculated from TB parameters of the metal [11, 22]. $\mathbf{A}$, being the self-interaction of the plane, is Hermitian. When a plane is not at the boundary, and so, both its neighboring planes are present, we have

$$\mathbf{B}^{\dagger}\mathbf{c}_{n-1}+\mathbf{A}\mathbf{c}_n+\mathbf{B}\mathbf{c}_{n+1}=0. \quad (2.31)$$

Since n is discrete, we use the Z transform [20]

$$\mathbf{F}(z)=\sum_n z^n\mathbf{c}_n, \quad (2.32)$$

where z is a complex variable, $\mathbf{F}(z)$ a column vector with J components. Only when z is of the form $\exp(i\theta)$ with real θ, does $\mathbf{F}(z)$ reduce to the familiar discrete Fourier

transform. From eqs 2.31 and 2.32 we see that

$$\mathbf{B}^\dagger \frac{\mathbf{F}(z)}{z} + \mathbf{A}\mathbf{F}(z) + \mathbf{B}\mathbf{F}(z)z = 0. \tag{2.33}$$

To obtain a nontrivial $\mathbf{F}(z)$ we set

$$\det\left(\frac{\mathbf{B}^\dagger}{z} + \mathbf{A} + \mathbf{B}z\right) = 0. \tag{2.34}$$

This equation has $2J$ roots. Taking the complex conjugate of the above equation to see the symmetry of the roots, we have

$$\det\left(\frac{\mathbf{B}}{z^*} + \mathbf{A}^\dagger + \mathbf{B}^\dagger z^*\right) = 0. \tag{2.35}$$

Since $\mathbf{A}$ is Hermitian, we see that if z is a root then $1/z^*$ is also a root and so the number of roots with $\mid z \mid < 1$ equals the number with $\mid z \mid > 1$.

The most general form of $\mathbf{c}_n$ is obtained by inverting the Z-transform (eq 2.32):

$$\mathbf{c}_n = \sum_m (z_m)^n a_m \mathbf{F}_m(z_m), \tag{2.36}$$

where the sum is over the number of roots $(2j)$, the z_m and $\mathbf{F}_m(z_m)$ are the eigenvalues and eigenvectors of eq 2.33, and the a_m can be determined from the boundary conditions and the normalization.

The boundary conditions are considered next:

1) **Bulk:** Any solution to eq 2.34, $z = z_m$, which has $\mid z_m \mid > 1$ or $\mid z_m \mid < 1$ will diverge at $+\infty$ or $-\infty$, respectively, and its a_m is set to 0. Therefore only $\mid z_m \mid = 1$ roots contribute to eq 2.36, so $z_m = \exp(ik_m)$ with real k_m [23], and there is a three-dimensional translational symmetry of the wave function. The final wave function is then of the form

$$\Psi_{\mathrm{k}}(\mathbf{r}) = \sum_{n,m,j} \exp(ink_m) a_m F_{m,j}(\exp(ink_m)) \Phi_j(\mathbf{r} - n\hat{\mathbf{R}}_{\mathrm{p}}), \tag{2.37}$$

where $F_{m,j}$ is the j^{th} component of $\mathbf{F}_m$ and the remaining a_m's can be determined by normalization. The number of $\Psi_{\rm k}$ equals the number of a_m's found from normalization. The number of $\Psi_{\rm k}$ also equals twice the number of bands present at that energy. Physically, these $\Psi_{\rm k}$ represent forward and backward propagating waves.

2) **Surface:** The crystal planes are denoted by $n = 1$ to $+\infty$. Two conditions are imposed on $\Psi_{\rm k}$:

(a) $\Psi_{\rm k}$ should not diverge at $n = +\infty$ and (b) $\mathbf{c}_0 = 0$, since there is no crystal plane there.

Condition (a) requires that only the $\mid z_m \mid \leq 1$ contribute to $\Psi_{\rm k}$. The a_m's associated with the $\mid z_m \mid > 1$ roots (the same in number as the $\mid z_m \mid < 1$ roots) are set to 0. Condition (b) requires that

$$\sum_{m,j} a_m F_{m,j}(z_m) = 0 \qquad (|z_m| \leq 1,\ j = 1\ to\ J). \tag{2.38}$$

To satisfy (b) we need at least as many solutions of eq 2.33 (i.e., z_m's) as there are orbitals (i.e., J or components of $\mathbf{c}_0$) and thus J of the a_m's are determined from the boundary condition. The most general form of the wave function is

$$\Psi_{\rm k}(\mathbf{r}) = \sum_{n=1}^{\infty} \sum_{m,j} (z_m)^n a_m F_{m,j}(z_m) \Phi_j(\mathbf{r} - n\hat{\mathbf{R}}_{\rm p}). \tag{2.39}$$

$\Psi_{\rm k}$ has two parts, one with $\mid z_m \mid = 1$, which propagates into the bulk, and one with contributions from $\mid z_m \mid < 1$, which approaches zero after a few layers [24]. In eq 2.39, J of the a_m are determined by the boundary condition, eq 2.38, and the remainder are determined by normalization. If l bands lie at the energy $\epsilon_{\rm F}$ (eq 2.25) then l solutions $\Psi_{\rm k}$ exist and l of the a_m need to be determined by the normalization.

Two special cases may arise:

(i) Due to the symmetry of the particular crystal (and the particular surface) under consideration none of the decaying solutions contribute to the wave function, e.g., as in the case of Au(111) modelled with only s-orbitals [26]. In this situation k and $-k$ (where $z = \exp(ik)$), both contribute to the wave function and a $\sin(nk)$-like wave

function (n being the nth layer from the origin) satisfies the boundary condition.
ii) At some particular values of $|\mathbf{k}_{\|}|$ (eq 2.22), no z with $\mid z \mid = 1$ will exist. In this case the boundary conditions may still be satisfied but the resulting wave function decays after a few layers, yielding a pure surface state.

In metals with a surface, the most common type of states are of the type given in eq 2.39. We use such states to calculate $\langle \Psi_{\mathrm{k}} | H | \Psi_{\mathrm{A}} \rangle$.

2.5 Calculation and results

The metals Au and Pt have very different densities of states at the Fermi level, the difference being largely due to the presence of the *d*-electron band in Pt. The values [11] of $\rho_{\mathrm{F}} = 2.20$/atom/eV for Pt and $\rho_{\mathrm{F}} = 0.29$/atom/eV for Au are used in the present calculation. The Fermi energies [11] of Pt and Au are taken to be 8.68 eV and 7.32 eV, respectively, and the lattice parameters [27] are 2.77 Å for Pt and 2.88 Å for Au. Literature values [11] of the TB parameters for the metals are used to calculate Ψ_{k}. These parameters were obtained by a fit to accurate band structure calculations. The extended Hückel theory is used to calculate the energy and overlap matrix elements of the bridge and the acceptor. The structure of the acceptor is estimated from the structure of X-ray data of similar compounds [28]. Only one alkanethiol chain is used instead of the entire monolayer. It was shown by comparison with added alkanethiol molecules that this approximation gave a reasonable and for our purposes adequate description of the coupling [13]. A parametrization of the bridge, and the sequential formula of Hsu and Marcus [13] were used to calculate the coupling element H_{kA}. The $|H_{kA}|^2$'s were averaged over 60 $\mathbf{k}$ vectors [29]. These $\mathbf{k}$ vectors were chosen randomly and included contributions from all bands. Thus, $|H_{kA}|^2$ is averaged over all bands and ρ_{F} is the total density of states. To make the calculations of Hsu one needs the difference in energies of a virtual superexchange state and the donor/acceptor state at the transition state. This difference can be calculated using a formula [30] given in ref [13].

Our result for the rate constants of the two metals for a 15 methylene unit alka-

nethiol monolayer gives a value of 1.8 for $k_{\mathrm{Pt}}/k_{\mathrm{Au}}$. This result is consistent with unpublished experiments [7, 8]. The ratio of the densities of electronic states of the two metals is 7.5.

The ratio of the exchange rate constants as a function of number of methylene units for the two metals is given in Fig. 2.2. The number of methylene units is varied from 3 to 20. This ratio gives the distance dependence of the *d*-orbital coupling. The overpotential dependence of the ratio is also calculated and is plotted in Fig. 2.3. The dependence is found assuming a value of 1.2 eV [31, 32] for λ. The same monolayer shields the acceptor in the solution from the metal surface, so we assume that the reorganization energy (λ) does not change on going from Au to Pt. To perform this calculation a value of 0.025 eV for k_BT, and the expression of the rate constant from eq 2.2 were used.

2.6 Discussion

It is seen both experimentally and theoretically that the nonadiabatic rate of electron transfer is not simply proportional to the total density of states. It depends instead on the density of states modulated by the the square of the coupling. Accordingly, it is necessary that the various bands from which the density of states arises be also considered.

A more detailed analysis of the results provides some insight into the nature of the similarity of electron transfer rates for Pt and Au, their large difference in density of states at the Fermi energy notwithstanding. With a density of states at the Fermi energy of 29.9 in no. of states/Rydberg/atom, the density of *sp* states of Pt is 0.6 and that of *d*-states is 29.3 [11]. With a density of states of 4.0 for Au at the Fermi energy, the density of *sp*-states was 1.6 and that of *d*-states was 2.4 [11]. From these results it can be inferred that while the *d*-states in Pt are not ineffective for coupling, their effectiveness is far below that of the *sp*-states. If for a rough estimate the ratio of individual coupling effectiveness of an *sp*-state and of a *d*-state in Pt were taken to be roughly the same as in Au, then the calculated ratio of 1.8 for the rate constants

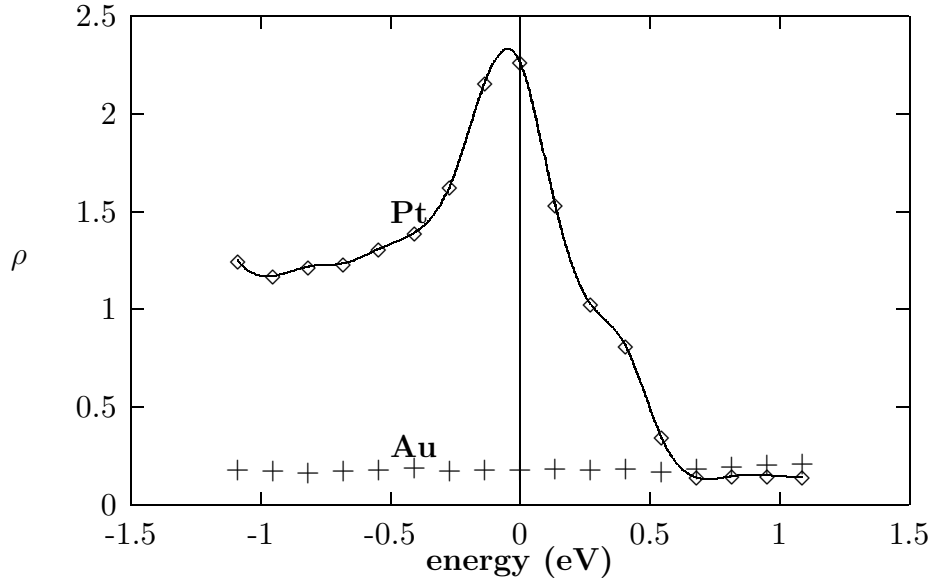

Figure 2.1: Band structure of Au and Pt with the Fermi energies of each set to 0. ρ is in units of no. of states per atom per eV. ($\diamond$) gives the density of states for Pt and (+) gives the density of states for Au.

leads from the above figures to a relative effectiveness of *sp*-states to *d* states of 11.2.

There has been some concern [33] that the extended Hückel method gives very narrow *d*-bands, which are more localized than in reality. In the present calculation, the metal is modelled using TB parameters which are not taken from extended Hückel and give good band structure results [11] (Fig. 2.1). The *d*-couplings we used for the Pt-S, Au-S and bridge-acceptor were however obtained from extended Hückel calculation using the standard parameters available with the program [12].

The fact that the *d*-orbitals are localized and not strongly coupled to the environment is well known from field emission experiments [36]. Thus, even though the *d*-electrons are present at the Fermi level they interact very weakly with external fields or ions and these electrons tunnel out from the metal much less than *s*-electrons at the same energy. This fact has been observed in field emission as well as in ion neutralization experiments [37]. It is thus perhaps, not surprising that this *d*-electron localization also manifests itself in a reduced contribution to the rate constant in electron transfer experiments.

The rate constants were calculated as a function of the number of methylene units

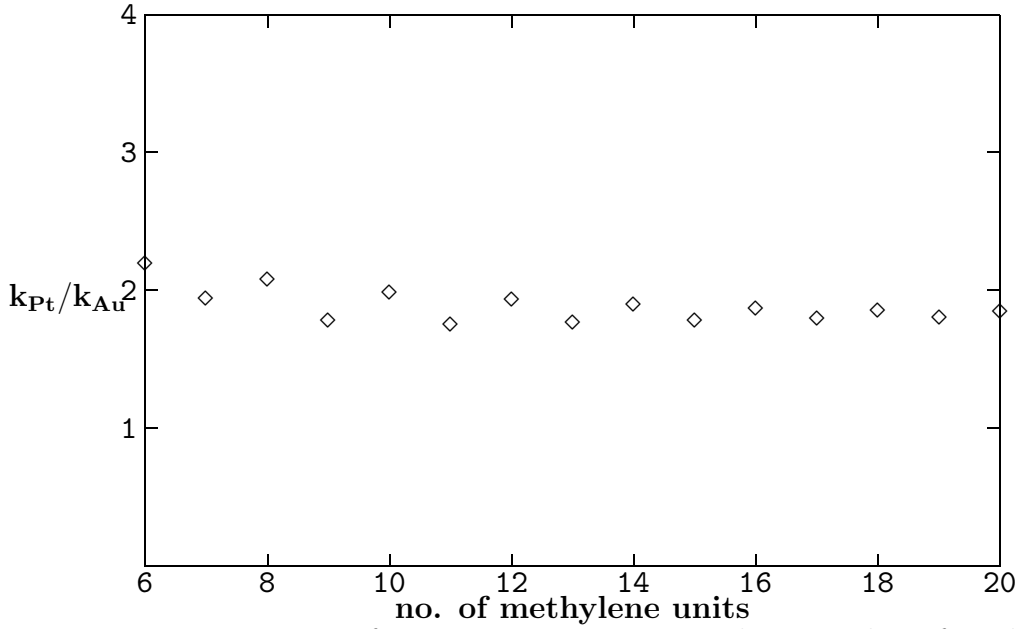

Figure 2.2: Ratio of rates at zero overpotential *vs.* number of methylene units.

for the two metals. Regarding the results in Fig. 2.2 we note that the ratio of the rate constants of Pt and Au changes little with number of methylene units.

We also calculate the overpotential dependence of the ratio of rate constants using eqs 2.2-2.5 (Fig. 2.3). We find that the ratio peaks close to the Fermi level and decreases weakly for positive overpotentials. This result is understood using the band structure of the two metals (Fig. 2.3): the density of electronic states of Pt is the highest close to Fermi level (zero overpotential), slopes gradually for negative energies relative to the Fermi energy and decreases sharply for positive energies while the density of states of Au is almost constant over the whole overpotential range. The change in ratio of rate constants with change in overpotential is very small for the anodic and cathodic parts of the curve. This small change should not cause any significant asymmetry in the rate *vs.* overpotential curves, because of the large direct effect of the overpotential in the exponent of eq 2.2.

The observation of the importance of the type of states for the present study rather than only the density of states has its counterpart in studies of intramolecular vibrational relaxation [34], where the total density of states does not play a direct role in the rate of relaxation. It is rather a local density of coupled vibrational states which is important. In surface physics, too, the concept of local density of states is

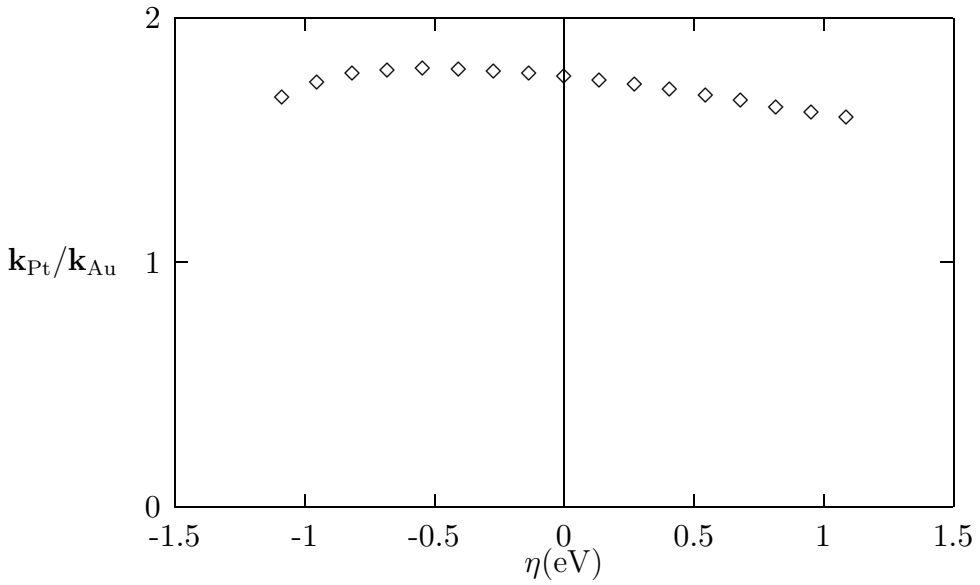

Figure 2.3: Ratio of k_{Pt} and k_{Au} *vs.* overpotential (η), assuming an equal λ for the two metals.

useful to understand spectra where contributions from different layers parallel to the surface might be different [35].

2.7 Conclusions

In this chapter, we have calculated the effect of the metal density of electronic states on the rate of electron transfer. We find that the rate constant is not simply proportional to the density of states. Instead, we need to consider the individual electronic coupling elements for each of the bands. The coupling matrix elements significantly reduce the effect of the extra density of states of weakly coupled bands, such as the d band. We find, consistent with electron emission results [36] and electron transfer experiments [7, 8], that the d band states couple weakly to the outside environment and thus, the rate constant for electron transfer does not reflect only the density of states.

Chapter 3

Temperature Dependence of the Electronic Factor in the Nonadiabatic Electron Transfer at Metal and Semiconductor Electrodes

3.1 Introduction

In this chapter, the temperature dependence of the electronic factor in the expression for the nonadabatic rate constant (k_{ET}) is discussed, both for metals and for semiconductors. In the case of the electrochemical exchange current at metal electrodes the temperature dependence of k_{ET} is due to two parts: one part arises from the well known variation with temperature of the Franck-Condon factor. It has an exponential term and a pre-exponential term which, classically, is proportional $T^{-1/2}$. The second part of the temperature variation arises from the increasing range of energies of electronic states in the metal near the Fermi level that can contribute significantly to the rate constant with increasing temperature. An experimental system of an alkanethiol monolayer adsorbed on two different metals, Au and Pt, is considered to investigate how this temperature dependence of the Fermi-Dirac distribution affects the rate. The metal electronic state dependence of the metal-reagent electronic coupling matrix element is included in the calculation. To a good approximation, the averaged electronic factor for the exchange current rate constant is calculated below to be proportional to T, the known proportionality when the electronic coupling element is energy-independent.

The temperature dependence of the electronic factor for nonadiabatic electron transfer at semiconductor electrodes is also discussed. For the present purpose, in lieu of detailed calculations, this factor is estimated using the free electron model. It is found to be proportional to the temperature T under conditions for the maximum of the rate constant, but the origin of the proportionality is quite different from that in the case of the electrochemical exchange current at metal electrodes.

In the following sections, the theoretical model used and the predictions that can be made from this model are described.

3.2 Theory

3.2.1 Metals

The rate constant for nonadiabatic electron transfer from a metal to a reactant at the interface (k_{ET}) is given by [17]

$$k_{ET} = \frac{2\pi}{\hbar} \int d\epsilon \; FC|V(\epsilon)|^2 f(\epsilon), \tag{3.1}$$

where $f(\epsilon)$ is the Fermi-Dirac distribution with ϵ measured relative to μ, the chemical potential of the electrons in the electrode,

$$f(\epsilon) = \frac{1}{1 + e^{\epsilon/k_B T}}. \tag{3.2}$$

FC is the Franck-Condon factor, which in its classical form is

$$FC = \frac{e^{-(\lambda - e\eta - \epsilon)^2/4\lambda k_B T}}{(4\pi\lambda k_B T)^{1/2}}. \tag{3.3}$$

Here, λ is the reorganization energy, e the electronic charge, η the overpotential, and $|V(\epsilon)|^2$ the square of the electronic coupling matrix element, integrated over the

distribution of the electronic states at the given ϵ:

$$|V(\epsilon)|^2 = \int d^3\mathbf{k}|H_{kA}|^2\delta(\epsilon(\mathbf{k}) - \epsilon), \tag{3.4}$$

where $|H_{kA}|$ denotes $\langle\Psi_{\rm k}|H|\Psi_{\rm A}\rangle$ and describes the electronic coupling between the redox agent (A) and each electronic state of wavevector $\mathbf{k}$ of the electrode.

Equations 3.1-3.4 are given for the reduction rate constant. The rate constant for the reverse reaction, which we will denote by k^r_{ET}, is obtained by replacing ϵ by $-\epsilon$ and η by $-\eta$. One can verify, for example, that the equilibrium constant k_{ET}/k^r_{ET} is then given by $\exp(e\eta/k_BT)$, as expected.

From eqs 3.1-3.3 we have

$$k_{ET} = \frac{2\pi}{\hbar}\frac{e^{-\lambda/4k_BT}}{(4\pi\lambda k_BT)^{1/2}}\int_{-\infty}^{\infty} e^{\frac{-\epsilon^2+h(\epsilon,\eta)}{4k_BT}} g(\epsilon)|V(\epsilon)|^2 d\epsilon, \tag{3.5}$$

where $g(\epsilon)$ is given by

$$g(\epsilon) = \frac{1}{2}\mathrm{sech}\left(\frac{\epsilon}{2k_BT}\right) \tag{3.6}$$

and

$$h(\epsilon,\eta) = 2(\lambda - \epsilon)e\eta - (e\eta)^2. \tag{3.7}$$

In applications, the dependence of $|V(\epsilon)|^2$ on ϵ is normally neglected. The reorganization energy λ is then obtained in two different ways, one from a plot of $\ln\ k_{ET}\ vs.\ \eta$ [38], and the other from a plot (noted below) involving $\ln(k^0/T^{1/2})\ vs.\ 1/T$, or both [39, 40]. While the effect of neglecting the dependence of $V(\epsilon)$ on ϵ is expected to be small, it is estimated in the present chapter. Results for finite η can also be estimated from the calculations, with appropriate additions, as discussed later.

When $\eta = 0$, eq 3.5 becomes k^0, the standard rate constant:

$$k^0 = \frac{2\pi}{\hbar}\frac{e^{-\lambda/4k_BT}}{(4\pi\lambda k_BT)^{1/2}}\int_{-\infty}^{\infty} e^{-\epsilon^2/4\lambda k_BT} g(\epsilon)|V(\epsilon)|^2 d\epsilon. \tag{3.8}$$

We first consider, for comparison, the simplest case: both the dependence of $V(\epsilon)$ on ϵ and the $\epsilon^2/4\lambda k_BT$ term in eq 3.8 are neglected. In that case the integral in eq 3.8

is a standard integral [41] yielding

$$k^0 \cong \frac{2\pi}{\hbar}\frac{e^{-\lambda/4k_BT}}{(4\pi\lambda k_BT)^{1/2}}\pi k_BT|V(0)|^2. \tag{3.9}$$

When the value of λ is obtained from eq 3.9 and a plot of the experimental rate constant k^0, $\ln(k^0/T^{1/2})$ *vs.* $1/T$, we have

$$\lambda/k_B = -4\ \partial\ln(k^0T^{-1/2})/\partial(1/T). \tag{3.10}$$

We next consider the case where the dependence of $|V(\epsilon)|^2$ is neglected, as before, but where the $\epsilon^2/4k_BT$ in eq 3.8 is included. In this case we have

$$k^0 \cong \frac{2\pi}{\hbar}\frac{e^{-\lambda/4k_BT}}{(4\pi\lambda k_BT)^{1/2}}\pi k_BT|V(0)|^2\langle e^{-\epsilon^2/4\lambda k_BT}\rangle, \tag{3.11}$$

where we have used [41] $\pi k_BT = \int_{-\infty}^{\infty} g(\epsilon)d\epsilon$ and where $\langle\rangle$ denotes an average over the distribution function, $g(\epsilon)d\epsilon/\int_{-\infty}^{\infty} g(\epsilon)d\epsilon$. The exponent is so small that the exponential in $\langle\rangle$ can be expanded, retaining only the first two terms. Use of standard integrals [41] then yields

$$k^0 = \frac{2\pi}{\hbar}\frac{e^{-\lambda/4k_BT}}{(4\pi\lambda k_BT)^{1/2}}\pi k_BT|V(0)|^2\left(1-\frac{\pi^2k_BT}{4\lambda}\right). \tag{3.12}$$

For a value [39] of $\lambda \cong 0.8$ eV and $k_BT \cong 0.025$ eV, the last factor in the parentheses, due to $\langle\exp(-\epsilon^2/4\lambda k_BT)\rangle$ term, is 0.923, and so is close to unity. In the following the $\exp(-\epsilon^2/4\lambda k_BT)$ in eq 3.8 will be replaced by unity.

In passing, we note that from eq 3.11 that the slope of $\ln(k^0(\lambda/k_BT)^{1/2})$ *vs.* λ/k_BT equals $-(1/4)(1-\pi^2(k_BT/\lambda)^2)$, because of the smallness of k_BT/λ. The reciprocal of this quantity can, because of the smallness of the correction, be written, as -4.04. A numerical evaluation of the integral [39] gave -4.03, which is within the round-off error. The difference of -4.03 from -4 is 1% and so can be neglected relative to other sources of error in λ.

The integral in eq 3.8 can now be written as

$$I(k_BT) = \int_{-\infty}^{\infty} g(\epsilon)|V(\epsilon)|^2 d\epsilon. \tag{3.13}$$

We have written the limits as $\pm\infty$, but of course the lower limit is finite. It equals the lower limit of the energy of the band, which is very negative. More than adequate for our purpose is changing the limits of integration to ± 1.1 eV.

The temperature dependence of $I(k_BT)$ arises from the weighting function, $g(\epsilon)$, which becomes broader with increasing temperature. The $|V(\epsilon)|^2$ depends only on ϵ and so is independent of temperature. However, because of the broadening of $g(\epsilon)$ with increasing T, parts of $|V(\epsilon)|^2$ at larger and smaller ϵ contribute more in the integral when the temperature is increased. For a $|V(\epsilon)|^2$ replaced by $|V(0)|^2$, the integral in eq 3.12, is, as already noted $|V(0)|^2\pi k_BT$.

For flat and broad bands, such as s and p bands, one expects $|V(\epsilon)|^2$ to remain constant with ϵ. In that case, the temperature dependence arises mainly from the width of the weighting function, $g(\epsilon)$, given in eq 3.6. For narrow bands, such as d bands, the density of states, ρ, changes fairly rapidly over a short energy range. If this feature leads to a large change in $|V(\epsilon)|^2$ then widely varying values of $|V(\epsilon)|^2$ become increasingly included in $I(k_BT)$ when the temperature is increased, and some deviation of the temperature dependence of $I(k_BT)$ from $|V(0)|^2\pi k_BT$ is expected. However, the d states do not couple as well into the donor/acceptor species in solution [42], the large change in the density of d states with ϵ is diminished by the small coupling of these states, so leading again to an approximately constant $|V(\epsilon)|^2$. In this case, the temperature dependence would remain about the same as in the case of the s and p bands, i.e., depend only on the width of the weighting function.

The accessible number of participating electronic states near the Fermi level ($\epsilon = 0$) increases linearly with temperature, a result well known from the proportionality of the electronic specific heat of the metals to the temperature. However, this observation offers no information on the average strength of $|H_{kA}|^2$ as a function of ϵ. The question of the behavior of the matrix element, suitably averaged, is

addressed in calculations in a later section.

Numerical results of the calculations based on eqs 3.4 and 3.8 (both with and without the $\epsilon^2/4\lambda k_B T$ neglected) are given in Section 3.3.

3.2.2 Semiconductors

In the case of electron transfer from a semiconductor to a reactant species in solution, the rate is first order in the concentration of electrons in the semiconductor at the surface and first order in the reactant. An expression for the second-order nonadiabatic rate constant k_{ET} was given earlier [43].

$$k_{ET} = \frac{2\pi}{\hbar}\frac{v}{\sqrt{4\pi\lambda k_B T}}\frac{1}{\beta_s}\frac{\int_0^\infty e^{-(\lambda+\Delta G^0-\epsilon)^2/4\lambda k_B T}\langle|\overline{V}(\epsilon)|^2\rangle e^{-\epsilon/k_B T}\rho(\epsilon)d\epsilon}{\int_0^\infty e^{-\epsilon/k_B T}\rho(\epsilon)d\epsilon}, \tag{3.14}$$

where $\langle|\overline{V}(\epsilon)|^2\rangle$ is an electronic matrix element [43]:

$$|\overline{V}(\epsilon)|^2 = \frac{|V(\epsilon)|^2}{\rho(\epsilon)} \tag{3.15}$$

and

$$\rho(\epsilon) = \int d^3\mathbf{k}\delta(\epsilon(\mathbf{k}) - \epsilon). \tag{3.16}$$

The average $\langle\rangle$ was over all orientations of the reactant at the contact distance [43]. In eq 3.14, v is the volume of the unit cell in the semiconductor (the wave functions appearing in $V(\epsilon)$ are normalized to that volume), and β_s is the exponent for the decay of the square of the matrix element with distance.

We note, in passing, that in the experiments [44], ΔG^0 is varied by varying the redox reagent in solution. The maximum k_{ET}, k_{ET}^{max}, determined in this way, corresponds to $\lambda + \Delta G^0 = 0$.

The exponent of the first factor in the integral in the numerator of eq 3.14 can be written as

$$\frac{(\lambda+\Delta G^0-\epsilon)^2}{4\lambda k_B T} = \frac{(\lambda+\Delta G^0)^2}{4\lambda k_B T} - \frac{(\lambda+\Delta G^0)\epsilon}{2\lambda k_B T} + \frac{\epsilon^2}{4\lambda k_B T}. \tag{3.17}$$

The first term in the RHS of the above equation is independent of ϵ and can be removed from the integral. The second term varies much more slowly with ϵ than the ϵ/k_BT in the exponent of the third term in the integral in eq 3.14, when $\lambda + \Delta G^0 \approx 0$ (the important region for k_{ET}^{max}, as noted above). The ratio of the third term in eq 3.17 to ϵ/k_BT is $\epsilon/4\lambda$, which is very small since $\epsilon \approx k_BT$, i.e., 0.025 eV, and λ is typically 1 eV. The dependence of $(\lambda + \Delta G^0 - \epsilon)^2$ on ϵ in eq 3.17 can then be ignored, yielding

$$k_{ET} = \frac{2\pi}{\hbar} \frac{v}{\sqrt{4\pi\lambda k_B T}} \frac{1}{\beta_s} e^{-(\lambda+\Delta G^0)^2/4\lambda k_B T} \frac{\int_0^\infty \langle|\overline{V}(\epsilon)|^2\rangle e^{-\epsilon/k_BT} \rho(\epsilon) d\epsilon}{\int_0^\infty e^{-\epsilon/k_BT} \rho(\epsilon) d\epsilon}, \tag{3.18}$$

as in eq A5 of ref [43]. Of particular interest is k_{ET}^{max}, which, obtained from eq 3.18, is

$$k_{ET}^{max} = \frac{2\pi}{\hbar} \frac{v}{\sqrt{4\pi\lambda k_B T}} \frac{1}{\beta_s} \frac{\int_0^\infty \langle|\overline{V}(\epsilon)|^2\rangle e^{-\epsilon/k_BT} \rho(\epsilon) d\epsilon}{\int_0^\infty e^{-\epsilon/k_BT} \rho(\epsilon) d\epsilon}. \tag{3.19}$$

When $|\lambda + \Delta G^0|/\lambda$ becomes different from zero, say, $\approx 1/2$, then the ratio of the second term in eq 3.17 to ϵ/k_BT becomes 1/4, which on integration including a slowly varying $\overline{V}(\epsilon)$ will affect the pre-exponential factor a little. The ratio of the last term in eq 3.17 to ϵ/k_BT becomes $\epsilon/4\lambda$, which for an averaged value of $\epsilon \approx \lambda/4$ in the sampling of ϵ's for the exothermic direction, is still a relatively small though not negligible quantity. Accordingly, eq 3.18 is expected to suffice for typical conditions. When it does not suffice eq 3.14 could be used instead. However, our main interest here is in k_{ET}^{max} and so in eq 3.19.

3.3 Applications

3.3.1 Metals

A particular system, an alkanethiol monolayer with 15 CH_2 units and with the redox agent $Ru(NH_3)_5Py^{2+}$ tethered to it is considered here. Only one alkanethiol molecule adsorbed on a metal electrode is used in our calculation, since it has been found that this approximation is reasonable, and adding more molecules does not have a large effect on the rate [13]. Two metals, gold (Au) and platinum (Pt), are considered, the

method of z-transforms and a tight binding Hamiltonian are used to obtain the wave functions of the metal. The details of the calculation are given elsewhere [42]. For the purpose of the calculations we use eqs 3.4, 3.15 and 3.16.

The metal Au has no d states near the Fermi level while the d band of Pt lies close to its Fermi level. The $\rho(\epsilon)$ given by eq 3.16 is plotted in Fig. 3.1 for both these metals, as well as the $g(\epsilon)$ at $T = 300K$. The Fermi levels of both metals are used as the zeros for their respective ϵ's.

The $|V(\epsilon)|^2$ is plotted in Fig. 3.2 for the two metals as a function of ϵ. It is seen that even though the $|V(\epsilon)|^2$ for Pt does change somewhat with the energy ϵ, the effect is considerably less than the change in $\rho(\epsilon)$. Although the extent of ϵ for which $g(\epsilon)$ is nonzero is $\sim \pm 0.3$ eV (Fig. 3.2) the validity of the $\lambda << \epsilon$ approximation and the neglect of the ϵ^2 term should be checked against the full width at half maximum of the $g(\epsilon)$ curve. The half-width is $\epsilon \sim 0.066$ eV. Thus, with the usual values of $\lambda = 0.6$ eV to 1.2 eV the approximation is still valid.

Although only a narrow range of ϵ is needed for our purpose of calculating the standard reduction rate constant k^0, we have given in Fig. 3.2 a substantially larger range of ϵ. When large overpotentials $\pm e\eta$ are considered, electronic energy levels with a correspondingly large range of ϵ are needed for the evaluation of the integral. Accordingly, this larger range of ϵ's is given in Fig. 3.2, should k_{ET} (or the reverse rate constant k^r_{ET}) at larger $|\eta|$'s, rather than just at $\eta = 0$, be needed. However, when large overpotentials are considered, the effect of the energy denominators should be included, e.g., [45].

The $\ln(I(k_BT))$ is plotted in Fig. 3.3 versus $\ln(k_BT)$ from $T \cong 120K$ to $T \cong 325K$ without and with the $\epsilon^2/4\lambda k_BT$. A value of 0.8 eV is used for λ. The slope is close to unity without the $\epsilon^2/4\lambda k_BT$ correction (1.00 for Au and 0.97 for Pt) and deviates a little from it with the correction (0.96 for Au and 0.93 for Pt). Thus, in both cases $I(k_BT) \propto k_BT$ is valid for the nonadiabatic electron transfer to Au and Pt. Accordingly, the temperature dependence of the electronic factor in eq 3.13 is proportional to T and so the k_{ET} in eqs 3.1-3.3 (apart from the exponential part of the Franck-Condon factor) is proportional to $T/T^{1/2}$, i.e., $T^{1/2}$. With the classical

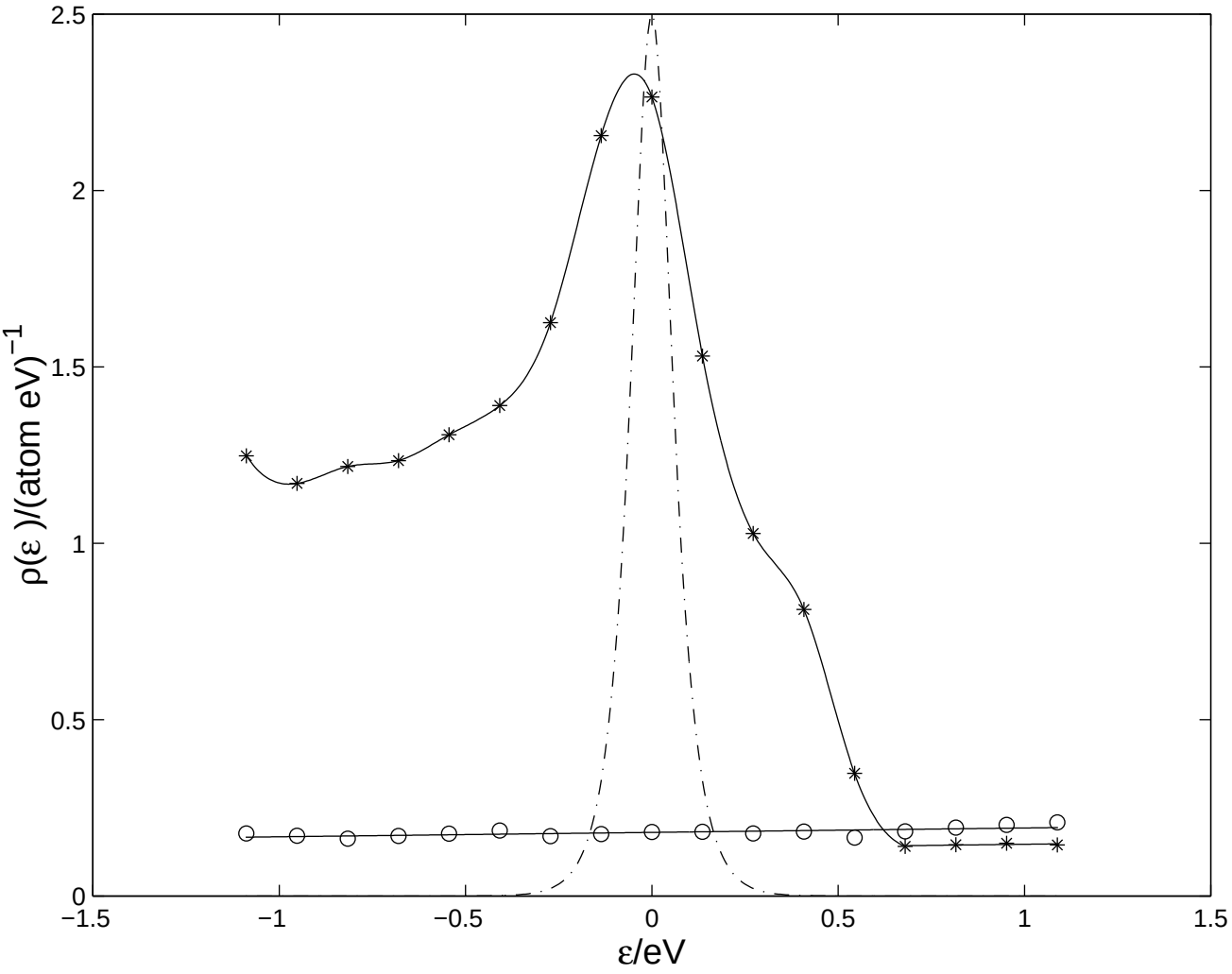

Figure 3.1: Band structure of Au and Pt with the Fermi energies of each set to 0. $*$ is for Pt and $\circ$ is for Au. $\rho(\epsilon)$ is in units of no. of states per atom per eV. The weighting function $g(\epsilon) \times 5$ at $k_B T = 0.025$ eV, i.e., $T = 300K$ is also plotted $(-\cdot)$ to show the density of states which contribute to the integral in the rate constant k_{ET}. For simplicity, a "splined" fit is drawn through the points for $\rho(\epsilon)$ for Pt.

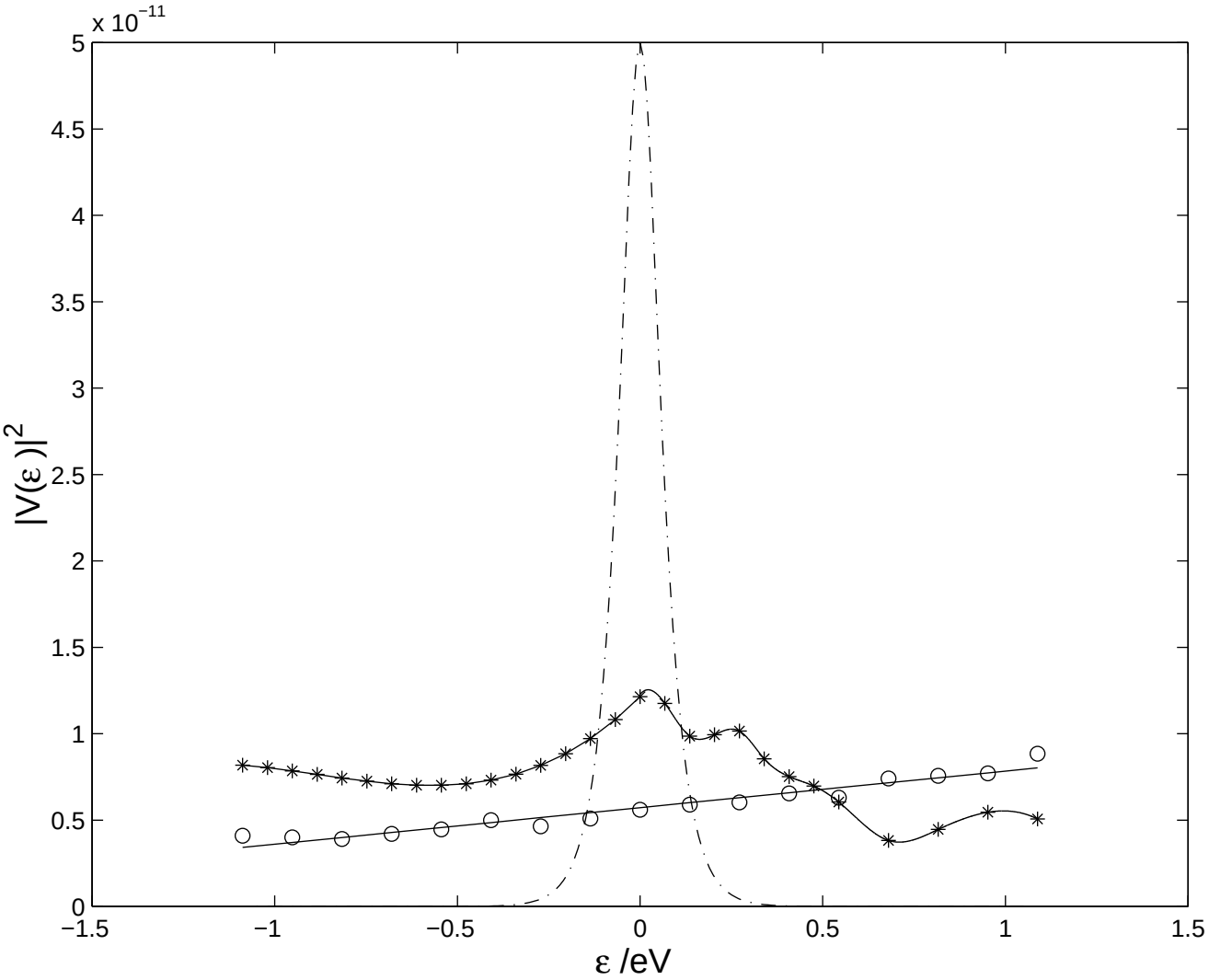

Figure 3.2: A plot of $|V(\epsilon)|^2$ *vs.* ϵ. $\circ$ gives the plot for Au and $*$ gives the plot for Pt. A plot of $g(\epsilon) \times 10^{-10}$ $(-\cdot)$ is also given. The Au curve is a best fit to the points, the Pt curve is a "splined" fit.

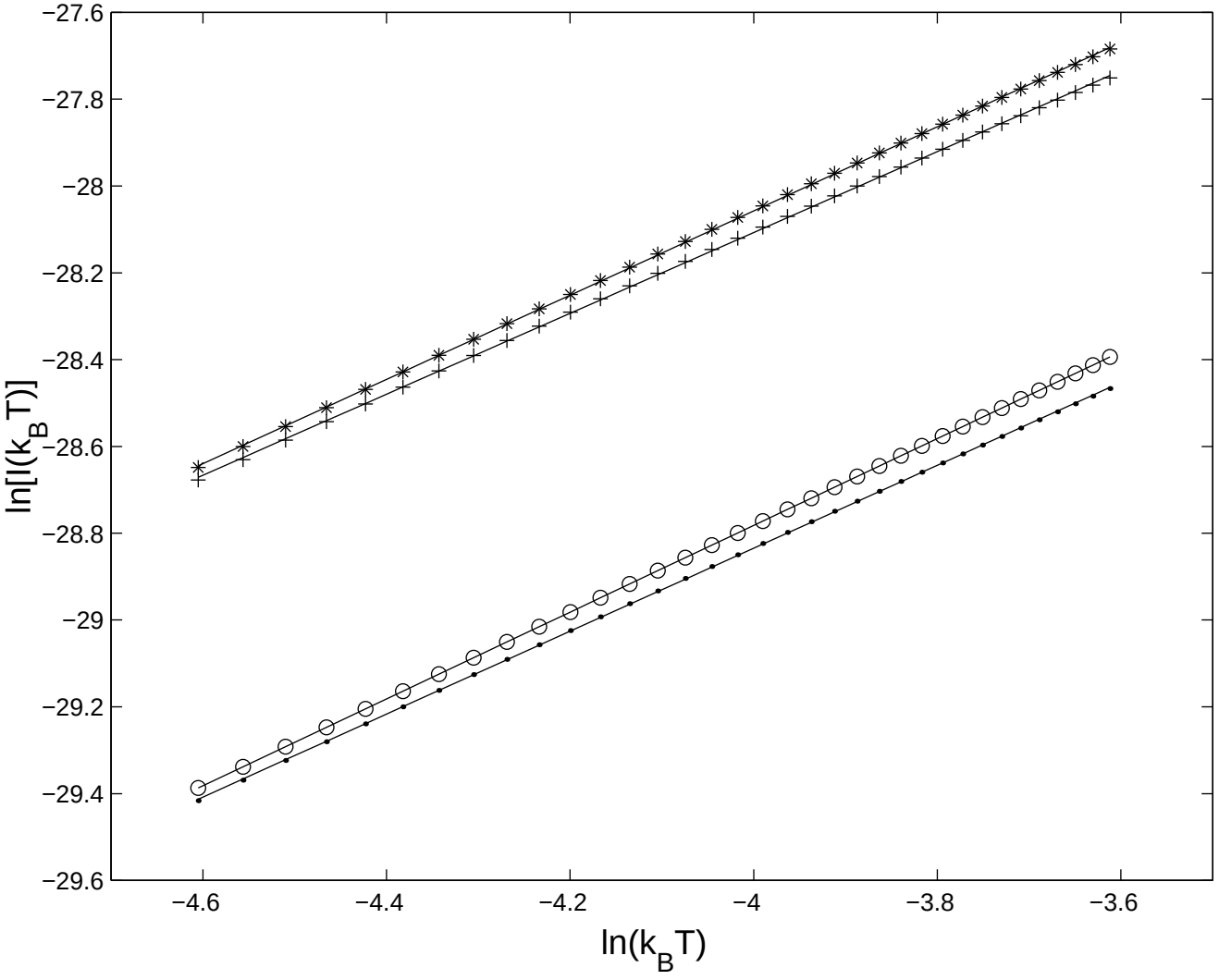

Figure 3.3: A plot of $\ln[I(k_BT)]$ *vs.* $\ln(k_BT)$. The slope gives the exponent of k_BT in $I(k_BT)$. The $*$ and $+$ (with the $\epsilon^2/4\lambda k_BT$ correction) points are for Pt and $\circ$ and $\cdot$ (with correction) points are for Au. The slope for Au is 1.00 and 0.96 (with correction) and the slope for Pt is 0.97 and 0.93 (with correction).

formulation for the Franck-Condon factor for the electrochemical exchange current, $k_{ET} \propto T^{1/2} e^{-\lambda/4k_BT}$ for both metals and thus we expect it to apply for other metals at these temperatures.

The slopes from Fig. 3.3 can be used to evaluate the value of the prefactor in eq 3.10. We proceed by writing the integral in eq 3.8 as $C(k_BT)^{1+\Delta n}$, where Δn is the deviation of the slope from unity and C is some constant. Equation 3.8 can then be written as,

$$k^0 = \frac{2\pi}{\hbar} \frac{e^{-\lambda/4k_BT}}{(4\pi\lambda k_BT)^{1/2}} C(k_BT)^{1+\Delta n}. \tag{3.20}$$

The above equation can then be used to find the value of $\partial \ln(k^0 T^{-1/2})/\partial(1/T)$. It equals $-\lambda/k_B[1/4 + \Delta n k_BT/\lambda]$, which gives instead of the factor of 4 in eq 3.10 a factor of $4/(1 + 4\Delta n k_BT/\lambda)$. For the slopes from Fig. 3.3, with $\lambda = 0.8$ eV and $k_BT = 0.025$ eV we get values of 4.02 and 4.04 for Pt (without and with $\epsilon^2/4\lambda k_BT$ correction) and 4.00 and 4.02 for Au (without and with correction).

The slopes of the $\ln(I(k_BT))$ *vs.* $\ln(k_BT)$ given above $(1 + \Delta n)$ could also have been obtained from an expansion of $|V(\epsilon)|^2$ in the vicinity of $\epsilon = 0$, using the data in Fig. 3.2.

$$|V(\epsilon)|^2 = |V(0)|^2 \left(1 + a\epsilon + b\epsilon^2 + c\epsilon^3 + d\epsilon^4 + ...\right) \tag{3.21}$$

The terms having odd powers of ϵ do not contribute, and so we have

$$I(k_BT) = |V(0)|^2 \pi k_BT \left[1 + (\pi k_BT)^2 b + 5(\pi k_BT)^4 d + ...\right]. \tag{3.22}$$

Since the $|V(\epsilon)|^2$ for Au is linear in ϵ at $\epsilon = 0$, (Fig. 3.2), b vanishes and it is clear why a plot of $\ln(I(k_BT))$ *vs.* $\ln(k_BT)$ was 1.00 for Au. Expanding $|V(\epsilon)|^2$ around $\epsilon = 0$ for Pt by fitting the Pt curve in Fig. 3.2 with various polynomial functions, it was found that the calculated slope varied from 0.9 to 1.0, thus yielding an almost linear plot [46].

3.3.2 Semiconductors

To treat the T dependence for semiconductor electrodes using eqs 3.18 or 3.19, calculations such as those given in ref [43] would need to be repeated at various temperatures. In the absence of those particular results we use here the free electron model [47] in which the matrix element H_{kA} (i.e., $\langle \Psi_{\rm k}|H|\Psi_{\rm A}\rangle$) at small ϵ is found to be proportional to $k_{\rm z}$ [48] (because $\Psi_{\rm k}$ is proportional to $k_{\rm z}$), and so $|H_{kA}|^2 \propto k_{\rm z}^2 \propto k^2/3 \propto \epsilon$, where ϵ is the energy. Since $\rho(\epsilon)$ varies as some (known) power of ϵ, one finds that the electronic factor, $\langle|\overline{V}(\epsilon)|^2\rangle$ in eq 3.14, is proportional to k_BT. A consequence is that k_{ET}^{max} varies as $T/T^{1/2}$, i.e., $T^{1/2}$.

3.4 Discussion

Two differences between metals and the present nondegenerate semiconductors may be noted: (1) In the former, the Fermi-Dirac distribution is needed, while the Boltzmann distribution suffices for the semiconductor. (2) As a first approximation the H_{kA} in eq 3.4, appearing via eq 3.15 in eq 3.19 for k_{ET}^{max}, is approximately proportional to $k_{\rm z}$ in the free electron model for the semiconductor [47]. Since $|\overline{V}(\epsilon)|^2$ is, as seen from above, proportional to $k_{\rm z}^2$ and since the transfer is from the edge of the conduction band, it is also proportional to ϵ. In the case of the metal, however, the distribution of the k's is hardly changed when the energy ϵ relative to the Fermi level is changed. Thus, now $|\overline{V}(\epsilon)|^2$ is essentially independent of ϵ. Specifically, at the high energies associated with k's near the Fermi level in free electron metals, $k_{\rm z}^2$ would be proportional to $(\Delta + \epsilon)$, where Δ is the energy of the Fermi level relative to that of the bottom of the band, namely about 2 or more eV. Thus, as ϵ is varied, the distribution of the $k_{\rm z}$'s is hardly changed, since $\Delta >> \epsilon$. This behavior is in marked contrast to that of the semiconductor at its band edge, where $k_{\rm z}^2 \propto \epsilon$.

These two effects, seen to be different for the semiconductor and the metal, nevertheless, for different reasons, gave rise to a proportionality of the electronic factor to k_BT for k_{ET} for the exchange current in the case of the metal and for k_{ET}^{max} in the

case of the maximum rate constant for the semiconductor.

Chapter 4

A Model for Charge Transfer Inverse Photoemission

4.1 Introduction

Inverse photoemission [49, 50, 51] has been extensively studied at the solid-vacuum interface and is used to map the empty electronic states in the band structures of metals. Several years ago, McIntyre and Sass [52] performed experiments at a metal-solution interface that were similar in nature to vacuum inverse photoemission spectroscopy (IPS). In their experiments, they used an electron transfer redox agent in solution to inject electons or holes into a metal electrode and create electronically excited states of the metal. These excited states decayed radiatively to give a spectrum. The competing nonradiative processes make the quantum yield of the emission very small. Because of the electrochemical nature of the experiments the redox agent-metal potential difference could be varied. The resulting light emission depended on the electrode-solution potential difference. This spectrum although low in intensity could in principle be analysed so as to provide information on the electronic structure of the metal above and below its Fermi level. The electrochemical experimental technique was termed charge transfer inverse photoemission spectroscopy (CTRIPS), and a schematic of charge transfer inverse photoemission is given in Fig. 4.1.

The purpose of the present chapter is twofold. There is a wide assortment of data though frequently no two laboratories have used conditions which serve as a check. We first assemble the available CTRIPS data and summarize the principal features

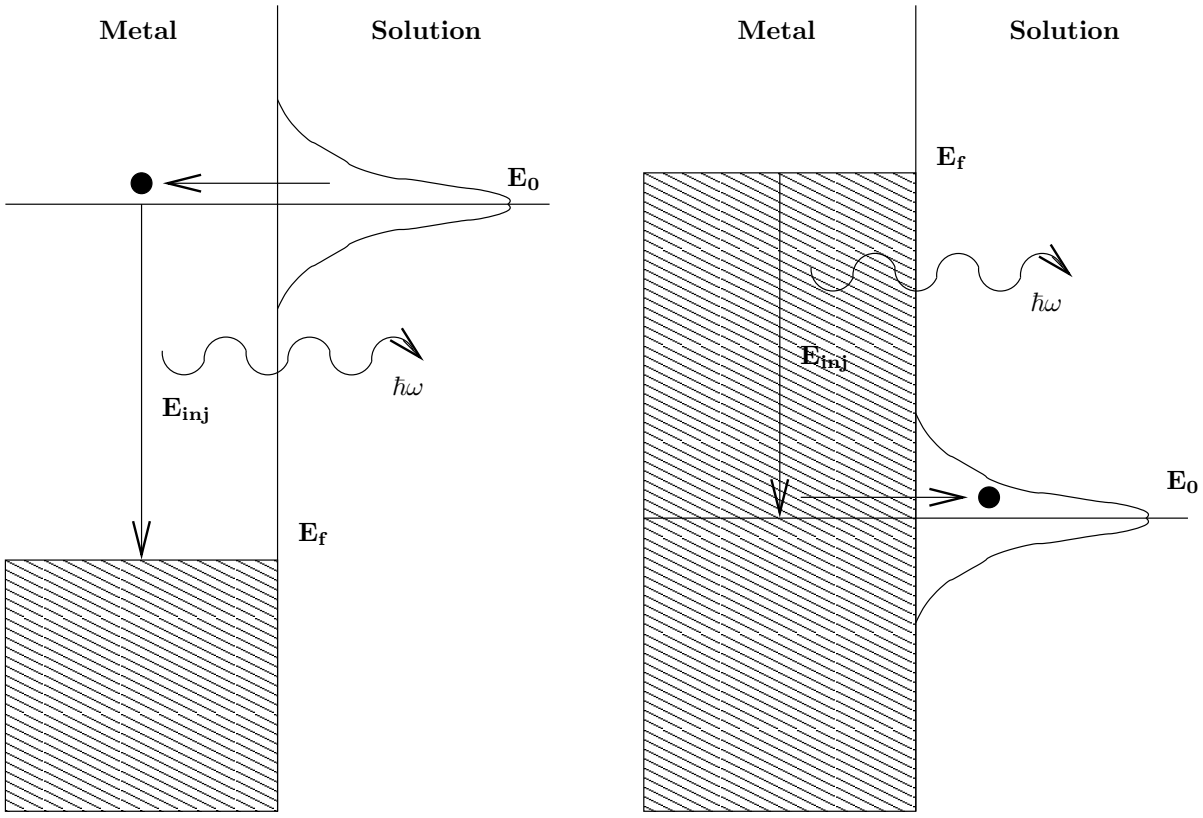

Figure 4.1: Schematic diagram for CTRIPS.

of the spectra. In the process we also note some inconsistencies in the data which need clarification.

A model is then presented for the electron transfer process and the light emission. A possible explanation of the data is given using the model and experimental band structures obtained from vacuum inverse photemission together with solution electroreflectance (ER) experiments. Several experimental tests of the model are also proposed, with the aim of clarifying further the various features of the spectra.

A simple model for vacuum inverse photoemission extensively used in the solid state physics literature [49] consists of three steps. (1) Electron injection into the metal, (2) electron transmission within the metal and relaxation of the electron by electron-electron collisions, and (3) emission of photons (mostly by direct vertical transitions). In this chapter we extend the above treatment so as to include in step (1) electron injection by electron transfer from a reactant to the metal and consider, too, the role of Franck-Condon factors in the initial electron transfer. The latter arise from the nuclear motion of the solvent as a result of the reaction satisfying the Franck-Condon principle [17]. Throughout the present chapter contact is made with the three-step model.

The difference between electron injection in vacuum and electron transfer in solution is that in the former case the electron is injected into a metal energy level above the vacuum level while in the latter both the energy level entered by the electron and the level to which it then falls lie below the vacuum level and above the Fermi level of the metal. Electronic levels above the vacuum level are free electron in nature and in the inverse photoemission experiments their character is assumed to be well known [49]. Thus, the spectrum elucidates the properties of the level to which the electron relaxes by photoemission.

In the solution experiments, in contrast, both the initial and the final energy levels are typically bound levels, i.e., below the work function threshold (vacuum level). Thus, the optical spectrum emitted in electrochemical inverse photoemission depends on the detailed band character of both levels. Since the energy difference between the two levels has a maximum of about 3.5 eV in most experiments, due

to solution stability constraints, it is not as large as in the vacuum experiments. It is expected from this energy difference that the final band into which the electron relaxes is close to the Fermi level of the metal and is the same irrespective of the energy level into which the electron (hole) initially enters, unless there is more than one band present at the Fermi level. Accordingly, it is expected that the change in the shape and position of the spectrum on changing the electrode/solution potential will be determined by the presence or absence of radiative bands at the electron injection energy and the nature of the states involved.

Electrochemical inverse photoemission spectra have been obtained with different metals, solvents, redox reagents, electrolytes, and electrode solution potential differences. The metals affect the spectra through their band structure, the solvent effect is due to a change in reorganization energy and the effect of different redox agents is due to their redox potentials (E_0). Since the potential of the electrode changes the positions of the the Fermi level (E_F) and bulk band energy levels of the metal electrode relative to the energy levels of the redox reagent (E_0), it strongly affects the emitted spectrum. Although temperature can have a substantial effect on photoemission, its effect on CTRIPS has apparently not been studied experimentally thus far.

The role of surface states in CTRIPS has been quite uncertain. In interpreting electroreflectance solution experiments [53], it was concluded that the surface states in a metal are in sufficiently close contact with the solution, that a change in the potential of the electrode does not affect them as much as it affects the bulk bands. The metal bulk band energies vary linearly with the electrode potential with a slope of 1 while the surface band energies might be totally pinned to the solution and so might not vary at all, depending on the conditions. In this case, the effect of varying the electrode potential in inverse photoemission depends on whether the emitting metal band states are surface states or bulk states. What is actually observed in each experiment should depend on the band structure of the metal and the electrode potential, and this aspect is included in treating the role of the band structure.

The spectra have in one instance been filtered into parallel and perpendicular

polarization components. They have also been measured at different emission angles. A comprehensive set of experiments of all types is not available for a single system or from a single laboratory, and so some "piecing together" of the diverse data is undertaken in the following section.

The chapter is subdivided as follows: In Section 4.2, the available experimental results are compiled and summarized. In Section 4.3, a model is suggested for their interpretation. The calculations and the results are described in Section 4.4 and discussed in Section 4.5. Experimental tests of the mechanism are proposed in Section 4.6.

4.2 Experimental results

Some of the principal observations made in the CTRIPS experiments are compiled and compared, and conclusions are drawn from these observations. Some results are replotted to make the comparison clearer. The experimental conditions used for different experiments are summarized in Table 4.1.

The earliest experiments on CTRIPS were those of Sass and McIntyre [52]. Their experiments were performed primarily using the gold electrode, acetronitrile as the solvent, and benzophenone as the redox reagent. They found that the high energy threshold (E_{th}) of the spectrum varies linearly with the potential of the electrode, E. The Fermi level of the metal E_F is pinned to the potential of the electrode E, and the two are used interchangeably henceforth. In a later paper [54] they found that E_{th} approximately equals E_{inj}, the energy above the Fermi level into which the electron is injected. This result is common to all the later experiments from all groups. E_{inj} equals $(E_F - E_0)$, E_0 being the standard potential of the redox agent measured on the same scale as E_F. They also observed in electron and hole transfer experiments [52, a] that the intensity of the hole transfer spectrum is about fifty times greater than that of the electron injection spectrum. They suggested that there were few upper radiative states available for the electron transfer step, due to a band gap at the Au(111) surface above the Fermi level, while the d-states present below the Fermi

Authors	**Solvent and Supporting Electrolyte**	**Donor/Acceptor, E_0 *vs.* Reference and *vs.* SCE in V**	**Metal**	**Reference Electrode**	**Voltage Range *vs.* Reference in V**	**E_{inj} Range in eV**
Sass and McIntyre '86	MeCN 0.5 M $TPABF_4$	Thianthrene +0.8, 1.18 Benzophenone -2.0, -1.62	Au(111)	$Ag/AgNO_3$ 10^{-3}M	(+0.9,-2.1) (-2.1,+0.9)	(-0.1, 2.9) (-0.1,2.9)
Ouyang and Bard '87	MeCN 0.1 M $TBABF_4$	Benzophenone -1.9, -1.9 *t*-Stilbene -2.17, -2.17 Benzonitrile -2.22, -2.22	Pt(111)/ polycrystalline Pt	SCE	(+0.2,+1.2) (-0.2,1.2) (-0.3,+1.2)	(2.1,3.1) (1.97,3.37) (1.92,3.42)
Ouyang and Bard '88	MeCN 0.1 M $TBABF_4$	Thianthrene +1.1, +1.1 Triphenylamine +1.1, +1.1 tris (2, 4 dibromophenyl)-amine +1.43, +1.43 9, 10 dibromo-anthracene +1.44, +1.44 Benzophenone -2.0, -2.0	Pt Pt/Rh	SCE	(+1.6,-1.4) (-2.5,+1.0)	(-0.5,2.5) (-0.5,2.5) (-0.17,2.83) (-0.16,2.84) (-0.5,3.0)
Uosaki, Murakoshi and Kita '91	MeCN 0.2 M $TBABF_4$	Benzophenone -2.15 -1.71 *t*-Stilbene -2.6, -2.16 Benzonitrile -2.7, -2.26	Au polycrystalline predominantly (111) faces	$Ag/AgNO_3$ 10^{-2}M	(-2.6,+0.7)	(-0.45,2.85) (0.0,3.3) (0.1,3.4)
Murakoshi and Uosaki '92	MeCN 0.2 M $TBABF_4$	Benzophenone -2.15, -1.71 *t*-Stilbene -2.6, -2.16 Benzonitrile -2.7, -2.26	Au and Pt and Pd predominantly (111) faces	$Ag/AgNO_3$ 10^{-2}M	(-0.5,+1.1)	(1.65,3.25) (2.1,3.7) (2.2,3.8)
Murakoshi and Uosaki '93	HMPA 0.2 M $NaClO_4$	solvated electron -3.4, -2.96	Au and Pt predominantly (111) faces	$Ag/AgNO_3$ 10^{-2}M	(-1.0,0.0)	(2.4,3.4)

Table 4.1: **A summary of the experimental conditions and voltages from various CTRIPS experiments.** A value of 0.38 V is added to convert from $Ag/AgNO_3(10^{-3}M)$ to SCE, and a value of 0.44 V is added to convert from $Ag/AgNO_3(10^{-2}M)$ to SCE. In Sass and McIntyre '86, the concentration of $TBABF_4$ is given as 0.5 M in the figures but 0.2 in the text. For light emission due to hole injection $E_{inj} = E_0 - E_F$.

level of Au(111) increased the intensity of the hole transfer. They also measured angle-dependent inverse photoemission [52, b] and polarization of emission [54, a] for Au(111). The detection of polarized light emission provides information about the optical matrix element of the radiative transition. The hole emission showed strongly p-polarised spectra which suggested an sp to d transition. They also compared their emission spectra from gold with that from silver [54, b].

Bard *et al.* presented results [55, 56] on the hole and electron transfer spectra at a platinum electrode, again using acetonitrile as the solvent. They also presented preliminary results using a rhodium electrode [56, a]. In their experiments they used a series of redox agents with different standard potentials and made a key observation: They observed a cutoff in redox potentials below which there was no light emission, this cutoff is denoted by $E_{R,th}$ for the electron injection and by $E_{O,th}$ for the hole injection. They proposed that this cutoff arises because of nonradiative Shockley surface states which are present above and below the Fermi level of platinum. They assumed that the surface states decayed in an efficient nonradiative process. On the other hand, if the injection is at an energy where no surface states are present, then a direct radiative transition was assumed to occur. From their hole and electron transfer experiments they calculated the band width of the Shockley states in platinum to be about 2.9 eV, which is similar to that obtained independently in solid state experiments [57].

Uosaki and coworkers described a number of experiments using a gold electrode, initially using acetonitrile as a solvent [58, 59] and later using solvated electrons in a hexamethylphosphoramide [60] (HMPA) solvent. In their measurements with the solvated electrons they again observed an $E_{th} \approx E_{inj}$, as well as a low energy threshold, E_l for the spectra.

In the initial study Uosaki *et al.* concluded that the light emission might involve surface states as acceptor states into which the electrons relax [58, a]. Subsequently [59], they compared the position of these surface states with positions of surface states observed in electroreflectance and concluded that surface states do not contribute to the spectrum, since they were already occupied at the potentials used

in the CTRIPS experiments. In another experiment [59], they measured the effect of electrode thickness on the intensity of light emission and observed that the spectral intensity increases with increasing electrode thickness [59, a], a result attributed to the increase in the number of bulk states with increasing thickness. This fact provided another basis for their conclusion that the bulk states contribute to emission intensity much more than do the surface states. They also compared the spectra from benzonitrile, t-stilbene and benzophenone at the same energy above the Fermi level (E_{inj}) [59, b]. Part of their figure is reproduced here in Fig. 4.2. It is seen that the spectra from benzophenone and benzonitrile overlap very well. Bulk states depend only on the potential of the electrode and thus the bulk band structure depends only on E_{inj}. From this fact and their data they concluded that the main contribution to the photoemission is from bulk states.

For comparison we have plotted in Fig. 4.3, a spectrum from Sass and McIntyre [52, c] for benzophenone together with one from Murakoshi and Uosaki [59, c] for benzonitrile, both at an E_{inj} of 2.9 eV. It is seen that the spectra do not coincide but rather there is a very large shift, so large that it may reflect a possible misprint in which one of the measurements may not have been converted to the appropriate relative electrode scale. The one difference in conditions in the two experiments is that of the supporting electrolyte which was the use of tetrapropyl ammonium fluoroborate ($TPABF_4$) for Sass and McIntyre and tetrabutyl ammonium fluoroborate ($TBABF_4$) for Uosaki *et al.* We discuss the effect of the supporting electrolyte and in particular the tetraalkyl ammonium ions [61] in Section 4.6.

Another consequence of the difference of supporting electrolytes, solvents, and references in the experiments of the various groups may lie in the difference in the measured E_0's of the redox couples [Table 4.1]. Problems may arise in the measurement of E_0 values in nonaqueous solvents due to liquid junction potentials [61]. To account for the differences in E_0 values we use energy differences in our calculations and comparisons and thus use E_{inj} (i.e., $E_F - E_0$) values [Fig. 4.1] wherever possible. To calculate these E_{inj} values we use the E_0 measured in the particular experiment.

Another pair [55, a][59, d] of spectra for platinum are compared in Fig. 4.4. The

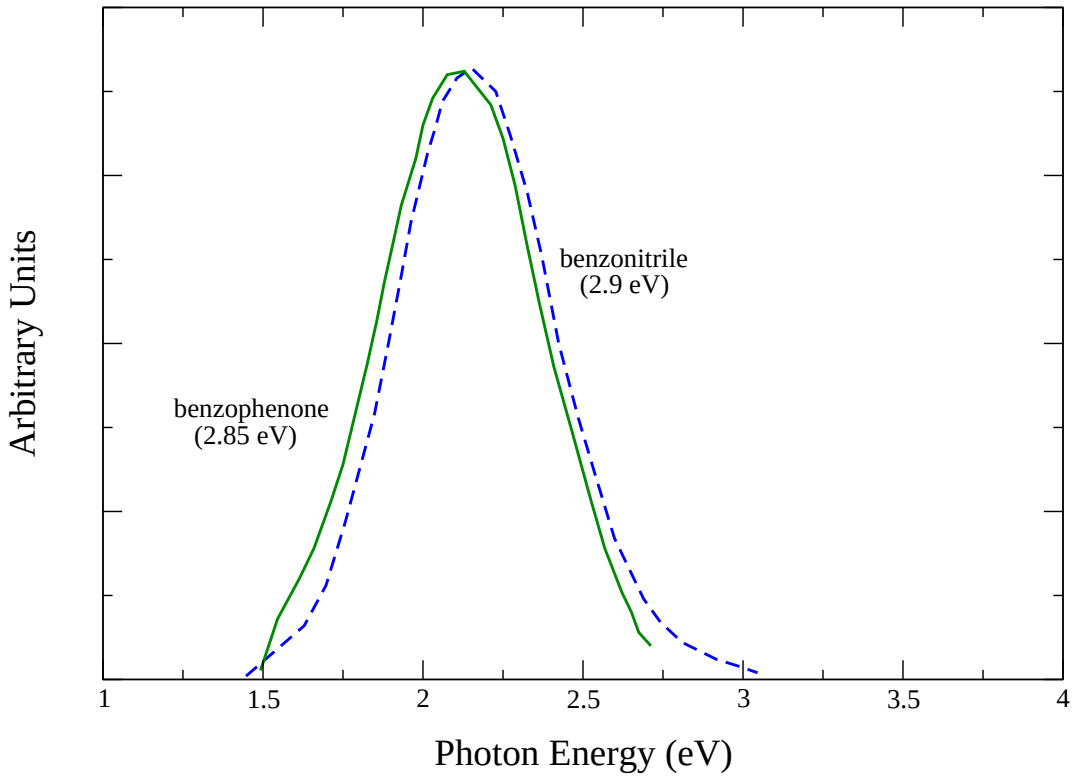

Figure 4.2: Inverse photoemission at Au(111) and constant $E_{inj} \approx 2.9\ eV$ using different redox agents. Results of Murakoshi and Uosaki [59].

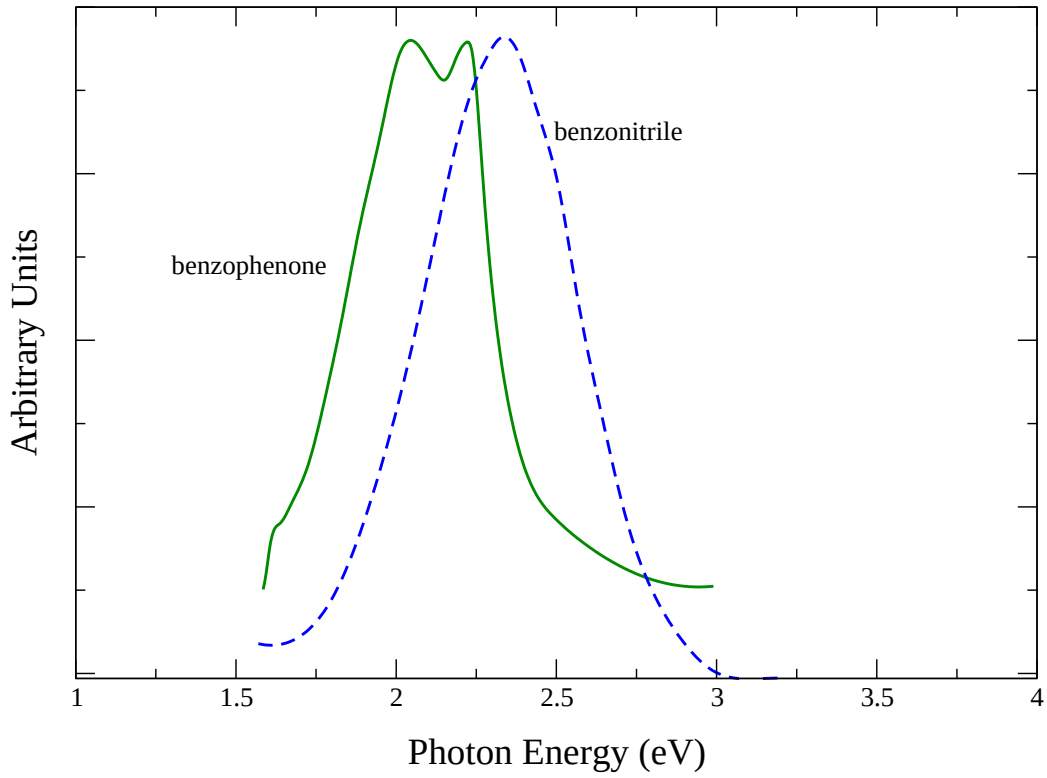

Figure 4.3: Inverse photoemission at Au(111) with constant $E_{inj} = 2.9\ eV$ using different redox agents. (- -) are the results of Murakoshi and Uosaki [59] and (—) are the results of McIntyre and Sass [52].

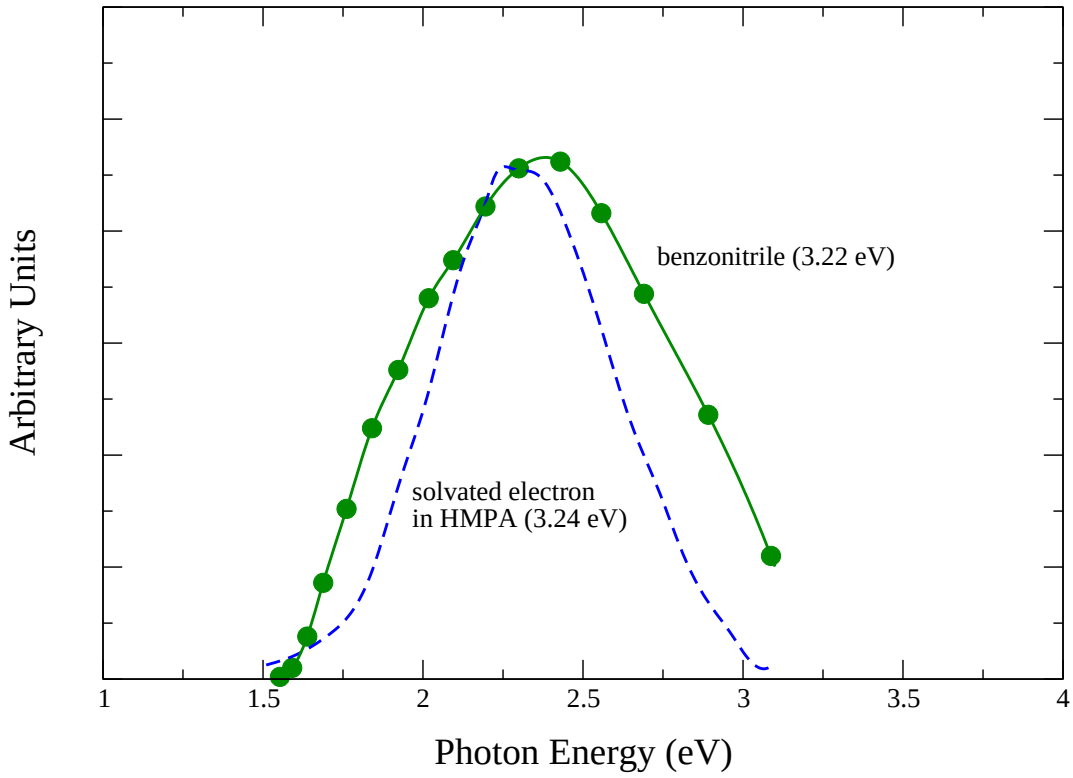

Figure 4.4: Inverse Photoemission at E_{inj} using different redox agents at the platinum electrode. (- -) are the results of Murakoshi and Uosaki [60] and (-•-) are the results of Ouyang and Bard [55].

spectra seem to have the same peak position but are shaped differently. While there is a difference in solvent (HMPA in the case of the solvated electron [55] and acetonitrile in the case of benzonitrile [59]), a repetition of each experiment in a single laboratory would be useful.

The spectra of Murakoshi and Uosaki, when plotted versus frequency [e.g., Fig. 4.2, Fig. 4.3, Fig. 4.4, Fig. 4.9], appear to be more symmetric than the emission spectra of the other two groups. It would be useful in future experiments to establish the exact shape of the spectrum as well as the frequency dependence of the spectra

at each energy excess ($E_F - E_0$). We also note that the plot of spectral emission *vs.* energy in the spectra of Murakoshi *et al.* is more asymmetric at high injection energies and tends to become symmetric at low injection energies [62, 63], principally because the low energy threshold is largely unaffected, but the high energy threshold shifts to the red when the driving force ($E_F - E_0$) is reduced. The shift with E_F is linear with unit slope.

Uosaki *et al.* plotted the quantum efficiency (Φ) for the benzophenone and benzonitrile [59, e] systems versus electrode potential. The curves look remarkably alike when the benzonitrile curve is shifted negatively by the difference in their standard electrode potentials. Thus, the shape of their spectra seem to depend only on E_{inj} values. They also plotted Φ for the solvated electron at gold and platinum electrodes [60, a], and found that the spectral intensity from platinum is much lower than that from gold. Unfortunately, none of the groups have compared the cutoffs from metals ($E_{R,th}$ or $E_{O,th}$) observed in the Bard group for Pt [55, 56] to see if they are different for different metals. In a later section we consider possible experiments which may clarify the existing results and provide further insight into the inverse photoemission process. There is a clear need for further experiments on the shape of the spectra, the dependence of the spectrum on the metal, the polarization of emitted light, the effect of the supporting electrolyte, the effect of temperature, and the appearance of the cutoffs $E_{R,th}$ and $E_{O,th}$ for different molecules and in different metals.

We suggest next a possible mechanism for CTRIPS.

4.3 Model

The model proposed here for the mechanism of CTRIPS with electron injection can be applied with minor changes to hole injection. We begin with the standard expression [64] for photon emission between two bands. It gives the intensity $I(\omega)$ in terms of the optical coupling between the two bands, V_{opt}, and the number of available

photon states ($\propto \omega^3$) at a given frequency ω:

$$I(\omega) = C\omega^3 |V_{opt}|^2, \tag{4.1}$$

where C is a numerical constant which depends on the dielectric constant ϵ_0, the speed of light c. The effective radiative coupling, V_{opt}, in the present case can be calculated using the three-step model. The ω is measured in units of energy (eV).

Step one of this model is the electron injection via an electron transfer to the metal. The expression for the first-order rate constant for a nonadiabatic electron transfer process [17] is given by

$$k_{ET} = \frac{2\pi}{\hbar} FC |H_{DA}|^2, \tag{4.2}$$

where FC is the classical expression for the Franck-Condon factor and H_{DA} is the electronic coupling between the donor and the acceptor. The first order rate constant to a redox molecule fixed at some position near the electrode. It is readily adapted to second-order constants [17, 66].

The metal electrode has a continuum of levels which contribute to the electron transfer process, each level in the metal being represented by a wave vector $\mathbf{k}$. For reactions at metal-solution interfaces the rate constant in eq 4.2 is used to include all the metal-reactant electron transfer energy states, obtained by integrating the right hand side of eq 4.2 over all energies ϵ and all $\mathbf{k}$ vectors contributing to a given energy. The energy, ϵ, is measured relative to the Fermi energy of the metal E_F. The rate constant for electron transfer is then given by [17]

$$k_{ET} = \frac{2\pi}{\hbar} \int d\epsilon \frac{e^{-(\lambda - e\eta + \epsilon)^2 / 4\lambda k_B T}}{(4\pi\lambda k_B T)^{1/2}} |V(\epsilon)|^2 f(\epsilon), \tag{4.3}$$

where the integration over wave vectors is included in the square of an averaged coupling matrix element, $|V(\epsilon)|^2$:

$$|V(\epsilon)|^2 = \int d^3\mathbf{k} |H_{Dk}|^2 \delta(\epsilon(\mathbf{k}) - \epsilon). \tag{4.4}$$

The $|H_{Dk}|$ is the electronic coupling between the donor (D) in solution and the quantum state of the metal represented by the wave vector $\mathbf{k}$, i.e., $\langle \Psi_{\mathrm{D}}|H|\Psi_{\mathrm{k}}\rangle$. Later, we will extend $|V(\epsilon)|^2$ to also include the coupling between the upper and lower metal electronic states contributing to photoemission. In eq 4.3, $f(\epsilon)$ is the Fermi-Dirac distribution with, as previously noted, ϵ measured relative to E_F, the Fermi level of the metal,

$$f(\epsilon) = \frac{e^{\epsilon/k_BT}}{1 + e^{\epsilon/k_BT}}. \tag{4.5}$$

In the present case the energy of the donor is much higher (> 2 eV) than the Fermi level, and $f(\epsilon)$ is essentially equal to 1. This substitution is made in the following calculations.

The FC in eq 4.2 is replaced by its classical expression,

$$FC = \frac{e^{-(\lambda - e\eta + \epsilon)^2/4\lambda k_BT}}{(4\pi\lambda k_BT)^{1/2}}, \tag{4.6}$$

where λ is the reorganization energy for the electron transfer, e the electronic charge, and $e\eta$ the overpotential equals $(E_F - E_0)$.

Thus far, we have included the effect of the electron transfer process in the expression for photoemission intensity. We need to consider in addition the details of the metal band structure, i.e., the energetic positions and the nature of the band into which the electron gets injected by electron transfer and the band to which the electron relaxes. Before proceeding to the band structure we need to ensure that the final state into which the electron relaxes is unoccupied.

To obtain the final intensity as a function of the overpotential, η one further term would be introduced, $f(\epsilon - \omega)$, which is the Fermi function for a final state. This term ensures that a final state into which the electron relaxes is unoccupied. The intensity is now given by

$$I(\eta, \omega) \propto \frac{2\pi}{\hbar} \int d\epsilon\ \omega^3 \frac{e^{-(\lambda - e\eta + \epsilon)^2/4\lambda k_BT}}{(4\pi\lambda k_BT)^{1/2}} |V(\epsilon)|^2 f(\epsilon - \omega), \tag{4.7}$$

where $|V(\epsilon)|^2$ is the coupling contribution from all the states which exist at ϵ in the

electronic band structure of the metal. The energy level of the metal, E_{inj}, above the Fermi level into which the electron is injected is the same as the overpotential $e\eta$. We assume initially, as in the above expression, that the optical absorption coefficient of the metal does not change the shape of the spectrum.

We now proceed to derive a detailed expression for $|V(\epsilon)|^2$ from eq 4.4. The inverse photoemission process in the three-step model is subdivided into electron transfer (step 1), electron relaxation by nonradiative (step 2) and radiative processes (step 3). We introduce this separation into the expression for $|V(\epsilon)|^2$. We begin with an expression very similar to the expression, eq 4.4, for pure electron transfer. Upon renaming the initial $\mathbf{k}$ by $\mathbf{k_1}$ and ϵ_k by ϵ_1, and so writing for direct transitions to state $\mathbf{k_2}$ in the metal, we have

$$|V(\epsilon)|^2 = \int\int d^3\mathbf{k_2} d^3\mathbf{k_1} |H_{Dk_1k_2}|^2 \delta(\epsilon_1 - \epsilon)\delta(\epsilon_1 - \hbar\omega - \epsilon_2), \tag{4.8}$$

where the second δ function arises from the conservation of energy during the photon emission. The $H_{Dk_1k_2}$ not only includes the H_{Dk_1} from eq 4.4 but also a term $H_{k_1k_2}$ of the form $\langle \Psi_{k_1} | T | \Psi_{k_2} \rangle$ describing the $\mathbf{k_1}$ to $\mathbf{k_2}$ transition, where T is the transition coupling operator. Thus,

$$H_{Dk_1k_2} = H_{Dk_1} H_{k_1k_2}. \tag{4.9}$$

The integration over $\mathbf{k_2}$ in eq 4.8 ensures that all possible final states are included.

To calculate H_{Dk_1} we introduce simple forms for the donor and metal wave functions. In a free-electron model the metal wave function would be of the form $Ae^{i\mathbf{k_1}\cdot\mathbf{r}}$. Since the metal has a surface, the above form is changed to one which satisfies boundary conditions at the surface, and the wave function becomes modified to [43] $Ae^{i(k_{1x}x + k_{1y}y)} \sin(k_{1z}z)$, where k_{1z} is the z-component of the wave vector of the metal. The simplest possible form [43] for H_{Dk_1} using this free electron model is $\sin(k_{1z}z)$. We also introduce a form for the wave function of the redox reagent and then calculate H_{Dk_1}. For simplicity, a spherically symmetric donor wave function (as is the case for a solvated electron) is introduced. A Gaussian form is assumed for this wave function, $B\exp(-(x^2 + y^2 + (z - z_0)^2)/(2\sigma^2))$, with σ being the mean radius of the donor and

z_0 the distance from the center of the donor to the the center of the metal atoms in the first layer of the electrode (one half lattice plane beyond the surface). In the case of a more complicated donor, an actual electron transfer matrix element should be calculated [47]. We expect that the final shape of the spectrum will not be substantially modified, because of the averaging over the various spatial configurations of the donor with respect to the metal.

The coupling can then be calculated assuming a constant coupling matrix element V, between the Gaussian donor and the sine-like metal wave function

$$|H_{Dk_1}|^2 = |V\ A\ B \int_{x,y=-\infty}^{\infty} \int_{z=0}^{\infty} e^{-\frac{x^2+y^2+(z-z_0)^2}{2\sigma^2}} e^{i(k_{1x}x+k_{1y}y)} \sin(k_{1z}z) dxdydz|^2. \quad (4.10)$$

The A and B are the constants from the assumed forms of the wave functions.

We next consider steps two and three of the three-step model, i.e., relaxation through radiative and nonradiative transitions. The radiative relaxation and resulting photon emission occurs due to an allowed coupling, usually transition dipolar in nature, between the initial and final electron states in the metal. This transition dipole coupling depends on the types of bands that exist in the metal. In our model we first assume for simplicity that this coupling is constant for all wave vectors and denote it by T.

The question of direct versus indirect optical transitions in the photon emission immediately arises. Direct transitions occur when there exist at least two accessible energy bands, an upper and a lower, at the given $\mathbf{k}$. In the case of a metal with a surface, only wave vector conservation of $\mathbf{k}_{\|}$, the component of the wave vector parallel to the surface, exists and a vertical transition occurs between the two accessible energy bands. When the transition arises from a wave function that is fairly deep in the metal, there is also an approximate conservation in the k_z component.

Indirect transitions also contribute to the photoemission and inverse photoemission processes in vacuum [49, 67], and are thus expected to play a role in CTRIPS. In the model, if direct transitions are not accessible then the electron can still radiate by indirect transitions.

There may also be a direct injection from the electron donor into some surface or bulk states which give rise to radiationless decay [55]. One reason why the surface states could be nonradiative lies in their band character. The surface state coupling is discussed in a later section.

We first calculate the contribution to $H_{k_1k_2}$ (eq 4.9) from direct transitions. As mentioned earlier, such transitions conserve $\mathbf{k}_\parallel$ during the photon emission. Using a two-band approximation for the band structure of the metal [Fig. 4.5] and the free electron model we obtain

$$|H_{k_1k_2}|^2 = \left| T \int_{-\infty}^{\infty} \int_{-\infty}^{\infty} \int_{z=0}^{\infty} e^{-ik_{1x}x + k_{1y}y} \sin(k_{1z}z) e^{ik_{2x}x + k_{2y}y} \sin(k_{2z}z) e^{-z/l} dx\ dy\ dz \right|^2 . \tag{4.11}$$

The l serves to introduce the relaxation of the electron through electron-electron collisions, l being the mean free path of the electron at the energy ϵ. $\mathbf{k}_\parallel$ is conserved and thus, the broadening is only introduced as an exponential in the z direction, $e^{-z/l}$, and not as an $e^{-r/l}$. The l also decorrelates k_{1z} from k_{2z} and serves as a measure of how different k_{1z} can be from k_{2z}. The integrals over x and y yield δ functions which give momentum conservation along $\mathbf{k}_\parallel$. The integral can then be performed.

We calculate next the contribution of indirect transitions to $H_{k_1k_2}$. If no direct transitions can occur then the electrons radiate only through indirect transitions. Photoemission caused by these transitions has been modelled quite rigorously [68]. In the present model, indirect transitions are introduced in a simple and quite approximate way. A broadening term similar to the mean free path broadening but present in all directions is introduced. This term, like the l of the direct transitions decorrelates the $\mathbf{k_1}$ from $\mathbf{k_2}$. A large broadening allows a calculation of $|H_{k_1k_2}|^2$, by an average integration of eq 4.11 to give a constant multiplied by T. This constant which we shall call T_{ind}, serves to reduce the entire spectral intensity of the indirect transitions relative to the direct ones. Upon introducing this approximation into the expression for the coupling, we have

$$|H_{k_1k_2}|^2 = T_{ind}^2 T^2, \tag{4.12}$$

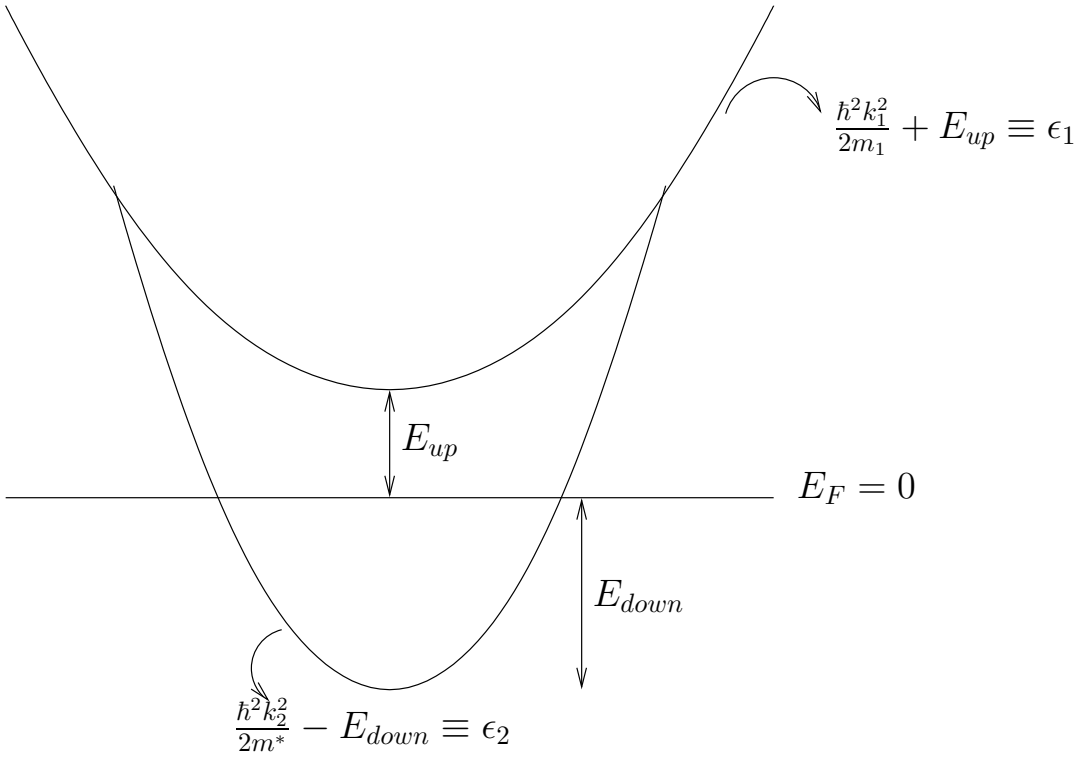

Figure 4.5: Two-band model for the band structure. The m^* and the m_1 are the effective masses of the electrons in the lower and the upper bands, respectively.

and so now the $|V(\epsilon)|^2$ for indirect transitions equals

$$|V(\epsilon)|^2 = T_{ind}^2 T^2 \int\int d^3\mathbf{k_2} d^3\mathbf{k_1} |H_{Dk_1}|^2 \delta(\epsilon_1(\mathbf{k_1}) - \epsilon)\delta(\epsilon_1(\mathbf{k_1}) - \hbar\omega - \epsilon_2(\mathbf{k_2})), \quad (4.13)$$

which is a product of the densities of states at the two energies ϵ_1 and ϵ_2, modulated by $|H_{Dk_1}|^2$.

We consider next the surface states, which in principle could be optically active or inactive. If they are optically active, they can be treated in the same way as bulk states with an extra broadening factor due to an effectively finite length of the states in the z direction. On the other hand, if they facilitate a competitive radiationless transition now they need to be introduced as sinks in the calculation, so preventing the electrons from radiating.

The position of the surface states with respect to the bulk states then needs to be calculated. It has been inferred from electroreflectance spectroscopy [73, 53, 69] that the position of the surface states depends strongly on the constituents in the solution. The surface states extend beyond the surface of the metal and any specific adsorption on the metal surface leads to a large change in potential at the surface. There have been several models of the double layer at the metal [70] and some of these models and simulation results [69] have been interpreted as indicating that the energetic position of the surface states can move as much as 1 eV/V with respect to the bulk states on changing electrode potential. This change in energetic position is attributed to specific adsorption. This movement implies that the bulk state potential is changed by changing the electrode potential while the surface states are pinned to the solution potential. In this case the difference of redox couple potential (E_0) and the surface state potential ($\equiv E_s$) remains approximately constant on changing the electrode potential. The surface states in the present model are positioned to reflect this behavior and are assumed to be dark states.

Equation 4.7 is evaluated using a Monte Carlo routine to obtain the light emission intensity.

In our calculations a model of the metal was used which fits the experimental band

structure measured by vacuum inverse photoemission. Surface state properties have been measured independently, and a linear dependence [73] of surface state energy on metal solution potential was used to locate the position of the surface states. Initially, with the assumption of optically inactive surface states, the experiment of McIntyre and Sass [52] was used to obtain the factor T_{ind} in eq 4.13. With these values the CTRIP spectrum was calculated and compared with experiment. The numerical values of the various parameters used and other details of the calculation and the results are given next.

4.4 Details of calculations and results

A spectrum for Au(111) is calculated using the above model. We consider the experiments of Uosaki and Murakoshi [60] which have a solvated electron as the donor and Au(111) as the electrode. The various properties used to describe the experiment include the vacuum band structure of Au(111), data from electroreflectance experiments, and adsorption studies with tetra alkyl ammonium ions. These data are given next.

The model for the band structure of gold is considered first. An experimentally measured (inverse photoemission) vacuum band structure [71] is given in Fig. 4.6. A particular cross section of the plot of $\mathbf{k}_{\|}$ *vs.* energy is shown there ($\mathbf{k}_{\|}$ has two components k_x and k_y). Three bands exist within the experimentally accessible range: a bulk band at about 3.6 eV above the Fermi level, a surface band which extends above the Fermi level, and another bulk band below the surface band. Our model for the metal is chosen to reproduce these bands of the spectrum. Gold has a face-centered cubic band structure, and in the experiments the (111) face is used. For simplicity, we assume a cubic band structure and a (100) face.

We first consider the bulk bands. The Fermi level of the metal is taken to be the zero of energy. The lower bulk band, ϵ_2 in Fig. 4.5, is modelled using the form $\hbar^2(k_x^2 + k_y^2 + k_z^2)/2m^* - 7.12\ eV$. The band gap in our model occurs due to a Brilliouin zone cutoff. m^* and m_1 are the effective masses of the electron in the lower and the upper

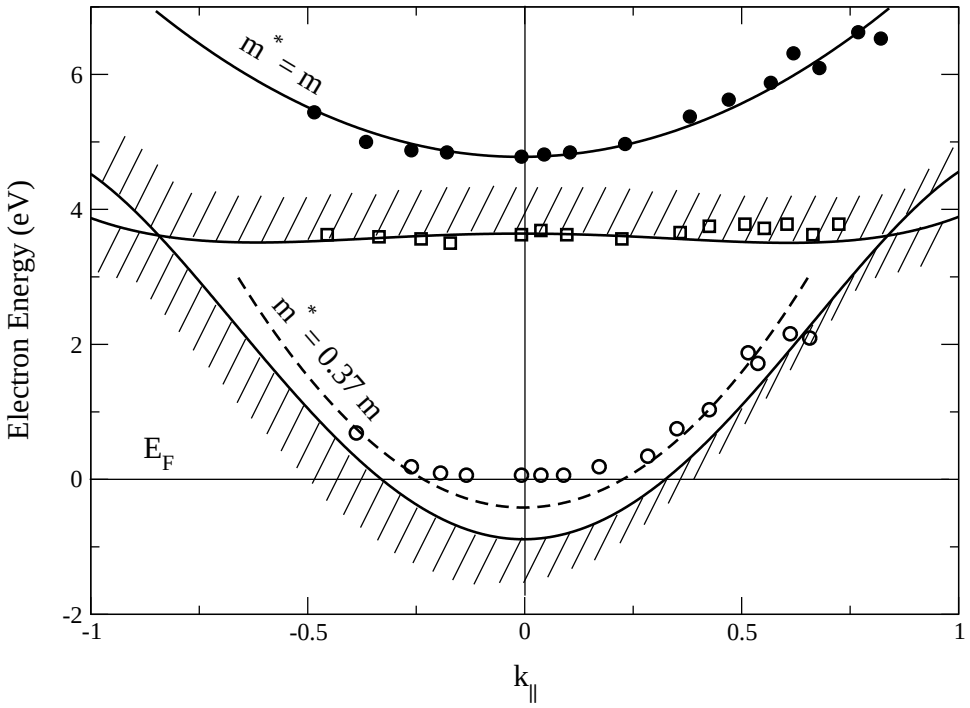

Figure 4.6: Measured band structure replotted from ref [71]. The symbols are experimental measurements. ○'s denote the lower band edge while □'s give the upper band edge. •'s give the image state. Hatching indicates the projected band structure. The dashed curve is the extrapolation of the dispersion relation obtained below E_F. The m^*'s are the effective masses of the electron in the given bands.

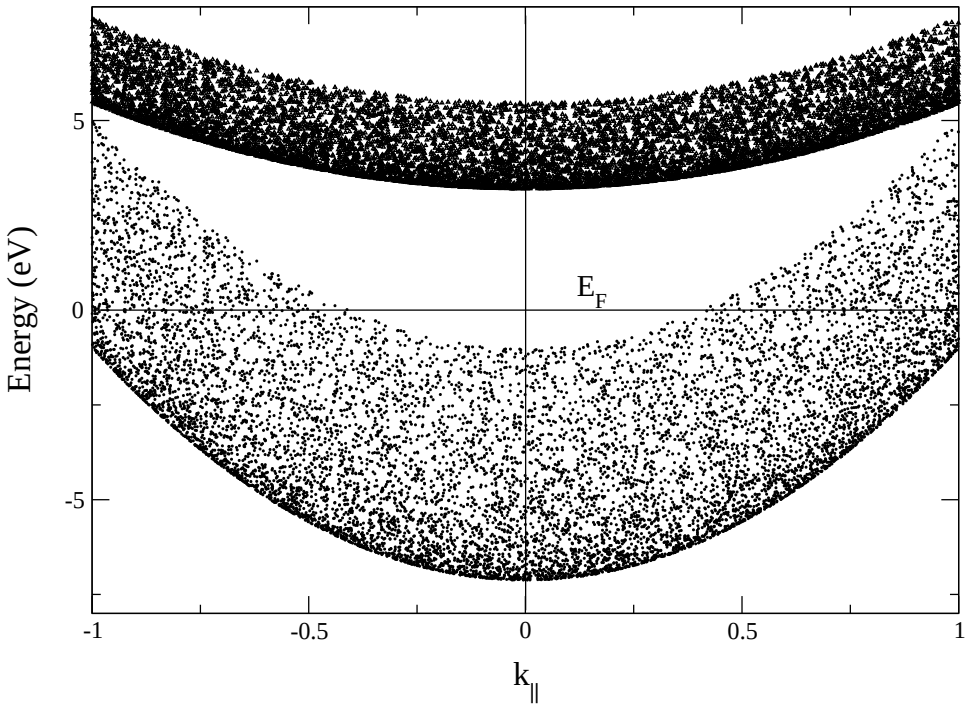

Figure 4.7: Projected band structure using the formulae for upper and lower bands given in the text.

bands, respectively, with $m^* = 0.37\ m$ and $m^* = 1.0\ m$, where m is the rest mass of the electron [71]. The upper bulk band is of the form $\hbar^2(k_x^2 + k_y^2 + k_z^2)/2m_1 + E_{up}\ eV$. A plot of the calculated band structure with $E_{up} = 3.2\ eV$ is given in Fig. 4.7.

We find that an $E_{up} = 3.2\ eV$ gives the best fit to experimental CTRIPS spectra for the values 3.6 eV, 3.4 eV and 3.2 eV. The band edge is observed to be located at 3.6 eV at the vacuum-Au(111) interface [71]. Band edges are fairly sensitive to the experimental conditions and might shift at the solution-metal inteface. This fact might be one of the reasons for the value of 3.2 eV giving the best fit. With the larger values of E_{up} that the transition between the indirect and direct represented, by the elbow shape of the calculated curve in Fig. 4.8 is more abrupt and the elbow gets sharper. This condition might also reflect the very approximate model that we use for the indirect transitions. The surface band is considered next.

The potential of zero charge (pzc), i.e. the electrode potential at which the elec-

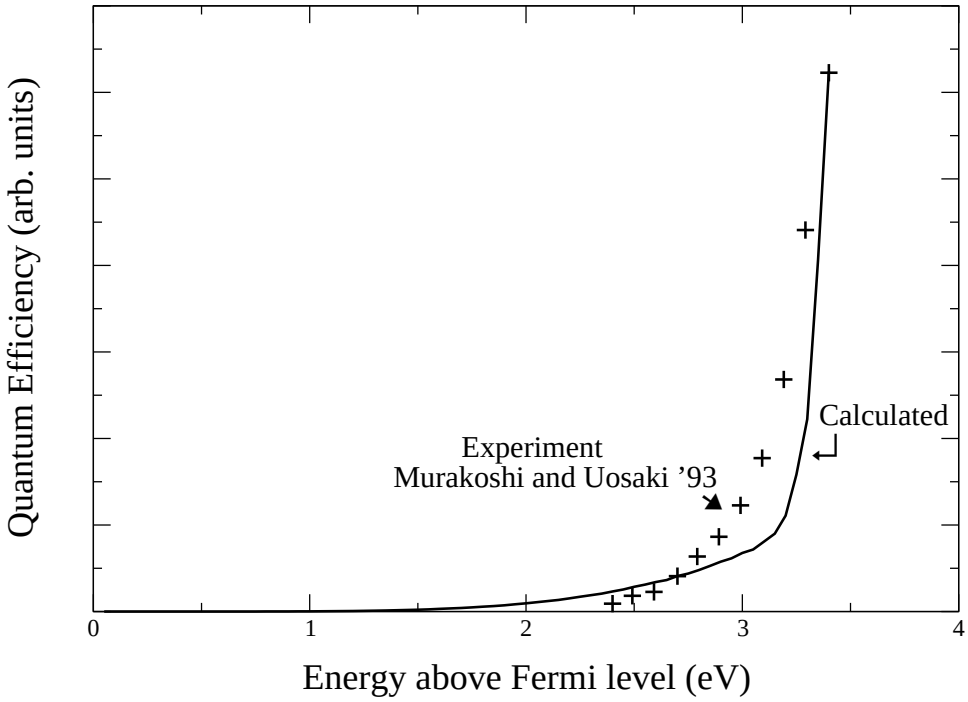

Figure 4.8: Quantum efficiency from Au(111) with solvated electrons. The +'s are experimental results replotted from Fig. 5 of ref [60]. The solid line (—) is calculated using the model in the present chapter.

trode is uncharged, plays a role in surface properties. When there are no adsorbed ions the double layer at the electrode is very diffuse. The band structure of the electrode (both bulk and surface bands) at the pzc is expected to resemble the vacuum band structure of the metal [69, 53, 70, 59]. The pzc [72] of Au(111) is 0.325 V with respect to the standard calomel electrode (SCE) while that of Pt(111) is 0.85 V. The energetic position of the surface band changes with respect to that of the bulk bands if the double layer structure at the interface is very dense, an effect which can be caused by the specific adsorption of cations or anions on the surface of the electrode [73]. The cations from most salts are small and highly solvated while the anions are large, with weak solvation shells and may adsorb. The supporting electrolyte in the case of the solvated electron experiments of Murakoshi and Uosaki is $NaClO_4$. The ClO_4^- ions are known to affect the surface states on Au(111) surfaces [73, 69]. We assume, as in ref [73], that the surface states vary at a slope of 1.0 eV/V on the positive charging side of pzc and at a slope of 0.2 eV/V on the negative charging side. Thus, the surface band is calculated using the formula $\hbar^2(k_x^2 + k_y^2)/2m^* - E_{surf}\ eV$, where the E_{surf} varies linearly with $E_F - E_0$ with the offset of the pzc and a slope of 1.0 eV/V on the positive side and a slope of 0.2 eV/V on the negative charging side. We remove an electron from our calculation if it enters the surface band. We use a $\lambda = 0.4\ eV$ for the solvated electron [60] and $k_BT = 0.025eV$.

The CTRIPS experiments [60] are performed by varying the electrode potential and thus E_{inj}, between 2.4 eV and 3.4 eV, and measuring the frequency-dependent spectrum at each of these voltages. The upper bulk band in the two-band model is at the edge of the experimental voltage. Also, from eq 4.7 we see that the peak of the spectrum will occur around the experimental voltage minus the reorganization energy, i.e., $(E_F - E_0) - \lambda$. As E_{inj} is lowered from 3.4 eV to 2.4 eV this band contributes less and less (proportional to the tail of a Gaussian) to the emission. Thus, direct transitions are possible only at the upper end of the experimental measurement. We assume a factor of 50 for T_{ind}, a factor inferred from the results on hole and electron spectra of Sass and McIntyre [52, 65]. The hole injection spectra of Sass and McIntyre are much more intense (by a factor of T_{ind}) than their electron injection

spectra. They explain this factor by considering the band structure of gold: There are no radiative states up to about 3 eV above the Fermi level in gold. Thus, they attribute their electron injection spectra to indirect transitions. There are radiative states present below the Fermi level and thus the hole injection occurs primarily by direct transitions. We adopt this explanation for the spectra and so calculate T_{ind}.

Some preliminary results from this model are given in Figs. 4.8 and 4.10. We reproduce the corresponding experimental spectra in Figs. 4.8 and 4.9. There is a fair agreement between the experimental and the theoretical results. We note that the treatment of indirect transitions in our model is only a first approximation, as reflected in the sharp transition from the direct to indirect transitions shown in the curves. The lower frequency cutoff arises from the approximate [43] $\sin(k_{1z}z)$ dependence of the matrix element and the shape of the band structure. The lower frequency cutoff occurs at a much higher energy ($\approx 1.5\ eV$) in the calculation of direct transitions. The addition of indirect transitions lowers it. The upper frequency cutoff arises because the Fermi level serves as the effective cutoff energy for the electron's radiative decay to the lower state.

4.5 Discussion

One principal question regarding CTRIPS is the role of surface states, namely whether they contribute to the spectra as radiative states or as sinks which facilitate radiationless (dark) transitions. Primarily because of the cutoff results of Bard and coworkers [55, 56], we feel the evidence currently favors surface states which facilitate radiationless transitions. In the present section we consider this point in the context of some experimental facts summarized below. We then give a possible mechanism which explains most of these facts in particular the cutoff of Bard and coworkers, and then briefly list a set of alternative mechanisms for inverse photoemission. These mechanisms may be useful to explain CTRIP spectra for metals with band structures different from Au or Pt. We also compare our model for photoemission with that of Murakoshi and Uosaki [60].

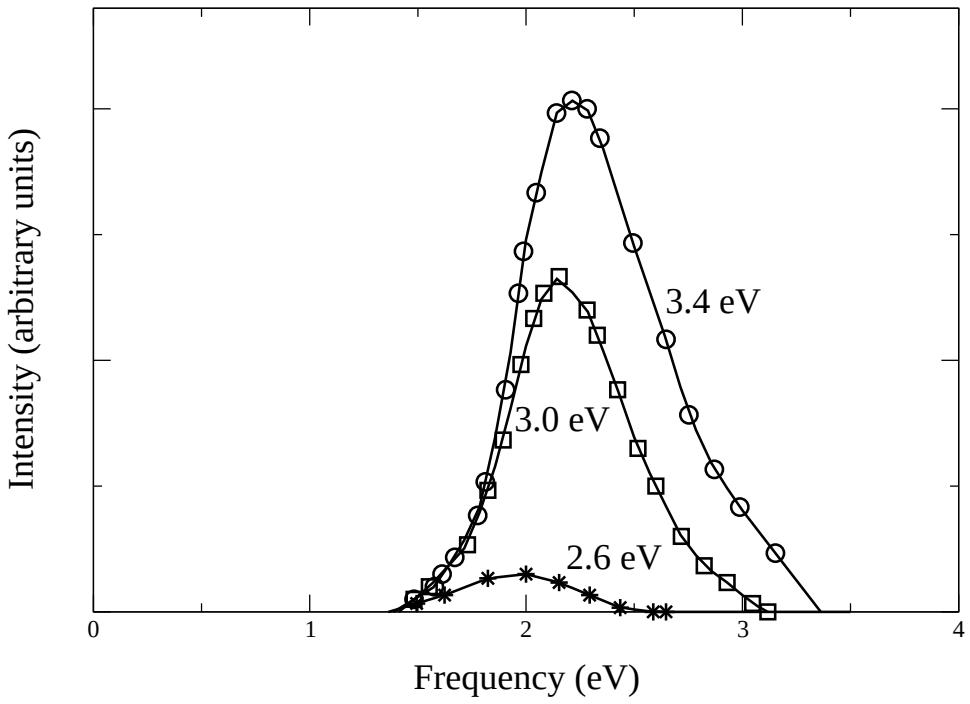

Figure 4.9: Emission intensity from Au(111) with solvated electrons. Replotted from Fig. 4 of ref [60].

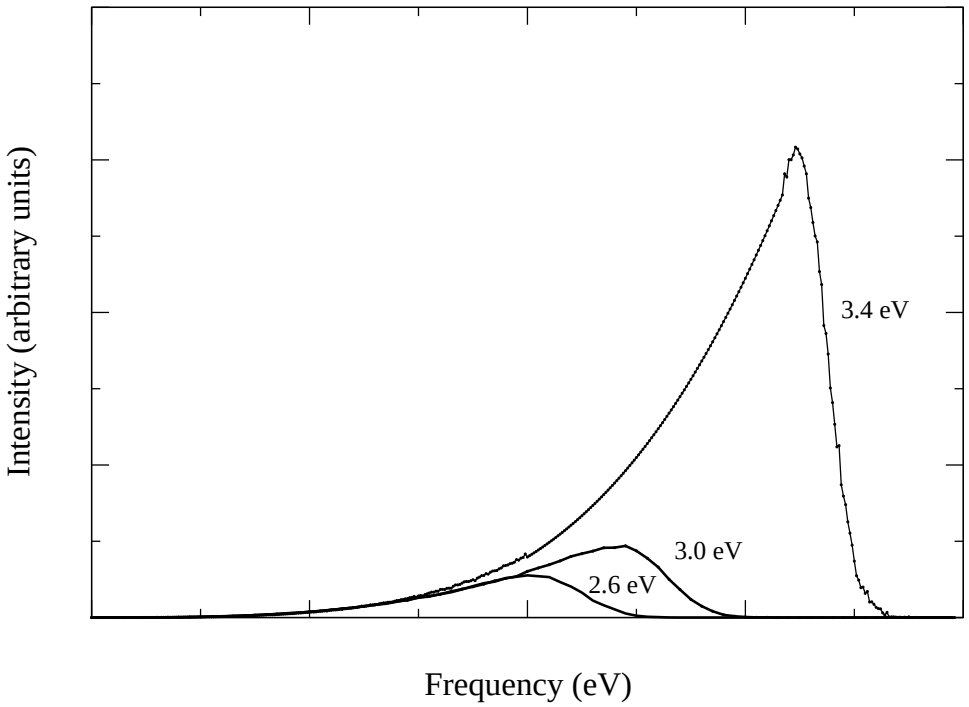

Figure 4.10: Light emission intensity from Au with Gaussian donor. Calculated using the model from Section 4.3.

Some key experimental results are summarized below. At present these results exist usually as isolated single-laboratory experiments and, as noted earlier, have largely not been yet repeated or tested in other laboratories.

1. The high energy edge of the emission spectrum varies linearly with potential, while the low energy edge is approximately potential independent.

2. There is a cutoff for the electron injection at Pt surfaces such that unless the standard potential E_0 of the donor is more negative than $-1.90\ V$ *vs.* SCE, the CTRIPS effect is absent, regardless of the driving potential, $E_F - E_0$. For hole injection at Pt surfaces, there is a cutoff such that unless E_0 of the acceptor is more positive than $+1.0\ V$ *vs.* SCE the CTRIPS effect again disappears.

3. The spectra arising at the Au(111) surface from hole transfer are fifty times more intense in a particular experiment than that from electron transfer.

4. The spectrum-integrated emission intensity increases sharply with electrode potential.

5. The emission intensity increases with metal film thickness at low film thicknesses.

6. Molecules having different E_0's have the same CTRIPS spectral plots, when they have the same driving potential $E - E_0$, provided the E_0 does not lie outside the cutoff region.

7. A decrease of the light emission yield when E exceeds a certain value has been observed [55, 59]. In ref [55] it occurs when $E > 1.2V$ relative to SCE, which translates to $E > 0.76V$ relative to Ag/Ag^+(0.01 M) standard used in ref [59]. This behavior is roughly consistent with the behavior in Fig. 7 of ref [59] for benzonitrile and a Pt electrode, where the decrease in emission begins around $E > 0.5V$ instead of $0.76V$.

The following mechanism is consistent with the above results: The electron is injected into a bulk state and decays radiatively to a bulk state. This decay yields the

emitted spectrum. If the electron is injected into a surface state, it decays nonradiatively. Surface states are thus assumed to be dark. They are assumed to be pinned to the surface if the supporting electrolyte shows specific adsorption.

In a bulk state to bulk state radiative decay, a change in a property, such as as film thickness, which affects the density of bulk states will cause a change in the spectrum, particularly in its intensity.

E_F changes linearly with electrode potential as do all the bulk state energies. Therefore, the spectrum will not change significantly with change of redox agent (E_0) if the electrode potential is changed in a way so as to compensate for a change of E_0, i.e., if $E_F - E_0$ is kept constant.

The optical matrix elements within the metal are such that the surface states become nonradiative. In the metals considered in this chapter (Au(111), Pt(111), etc.), only Shockley surface states (and not image states) have been reported within the energy range of interest above the Fermi level [57]. The Shockley states are intrinsic surface states formed due to the abrupt ending of the metal at $z = 0$. These states are of the same electronic character as the band that they arise from, a band which is primarily *sp* in character in the present instance. An electron may decay from an *sp* bulk band to the *sp* surface band radiatively because of symmetry breaking in the direction of the surface, i.e., the z direction. Alternatively, the band character of both bands being *sp*, this transition may be largely optically forbidden but nonradiatively allowed, and so the electrons may decay nonradiatively through these surface states. In some recent calculations [74] in Pt(111), it was observed that the *d*-states were squeezed out of the first layers near the surface. This circumstance might lead to a smaller optical matrix element between bulk *d*-states and the predominantly *sp* surface states in the first few layers of the crystal causing the surface states to be dark for electron injection Pt(111).

As noted earlier the thickness-dependent experiments of Uosaki and Murakoshi [59] suggest that the band into which the electron is injected is likely to be bulk band. In the case of Au(111) there is only one bulk band present up to about 3.4 eV, rather than an unoccupied upper and an unoccupied lower band required for light emission.

The experiments of Uosaki and Murakoshi [58] nevertheless show that there exists a spectrum at E_{inj}'s in the range 2.4 eV to 3.4 eV above E_F. Such a spectrum can arise, in principle, from an indirect transition.

In Pt(111), the band structure is such that the cutoff in emission spectra [55] can only be explained by the presence of nonradative surface states which are also stationary with respect to the energy of the redox couple. This behavior can only happen if the surface states stay pinned to the solution potential while the bulk states move linearly with the electrode potential. That is, the surface states would move linearly with respect to the bulk states with a slope of 1.0 eV/V on changing electrode potential. Such behavior is observed on the positive charging side of the Au(111) [53, 69] due to the specific adsorption of the anion. The pzc of Pt(111) is 0.085 V *vs.* SCE, as noted earlier, when the electrolyte is $HClO_4$. The region of experiments is 0.22 to 1.44 V *vs.* SCE. The supporting electrolyte used in the experiments of Bard and coworkers [55, 56], is $TBABF_4$. The tetrabutyl ammonium ions are known to specifically adsorb on metal surfaces [61, 75]. To explain the data of Bard and coworkers [55, 56] it is necessary to assume that this adsorption is the cause of a slope of 1.0 eV/V for the change of the surface band energy with respect to the electrode potential on the negative charging side of the electrode. Specific adsorption also changes the pzc and thus it is necessary for a clearer interpretation that both the electroreflectance experiments and the CTRIPS experiments be conducted with the same supporting electrolyte, such as $TBABF_4$. Light emission spectra calculated using the model presented here become more symmetric and show a peak shift to lower energies with an increase in λ values.

Two other mechanisms for radiative transitions which could also give rise to light emission are listed next. These mechanisms could contribute to emission at other metals with different band structures. Reasons are given for their not contributing to the spectra in the case of Au/Pt/Pd.

1. The electron is injected into a surface state and emits radiatively, so reaching a lower unoccupied bulk state. The position of the state into which the electron is injected may change with potential under particular circumstances [69] since

it is a surface state. The relative position of the surface and bulk states changes approximately linearly with potential, and the spectrum changes accordingly. However, since the surface states on the (111) face of both Pt and Au are low in energy [57], it is unlikely that they would contribute to the spectra as injection states.

2. The electron is injected into a bulk state and decays radiatively from the bulk state to a surface state. A change in any property which affects the density of bulk states, such as the electrode thickness, causes a change in the properties of the spectrum, such as intensity. Also, the spectrum changes with potential because of the relative shifts in energies as before. This mechanism cannot be used to explain the Pt(111) cutoffs of Bard *et al.* [55, 56] which requires sink states which remain stationary when the electrode potential is changed. In Au(111), on the other hand, the surface states are occupied if one assumes specific adsorption. Thus, the surface states are not available for relaxation and light emission, and so such a mechanism is not considered further.

In concluding this section we briefly compare our model with that of Murakoshi and Uosaki [60]. Both are three-step models. Three-step models are approximations to one-step models [50] of inverse photoemission which describe an overlap between the electron transfer state outside the metal and the final state after photon emission. Murakoshi and Uosaki describe the relaxation processes (step two of the three-step model) more rigorously than the present chapter, which introduces electron-electron collisions through a single relaxation length parameter. Also, the present chapter neglects any reabsorption of emitted photons which is treated in ref [60].

However, in the present chapter we present a model which uses actual expressions for electron transfer into the metal. We assume that if direct transitions are possible, then the bulk of the photoemission intensity arises due to $\mathbf{k}_{\|}$-conserving transitions. If direct transitions are not possible, then we invoke indirect transitions.

The model in ref [60] treats the electron transfer step using a constant energy independent tunnelling probability. The model also assumes no $\mathbf{k}_{\|}$ conservation and

so no possibility of a direct transition. All the spectral intensity arises due to indirect transitions and so the band structure information is introduced into the problem only through the density of states in the metal at a given energy. Information about band gaps is lost in this way. Direct transitions and $\mathbf{k}_{\|}$-conservation play a major role in inverse photoemission in vacuum at low energies and so are expected to play some role in CTRIPS too. The overall shape of the spectra calculated in the present chapter remains approximately the same as that calculated in ref [60]. However, using an expression for electron transfer and the band structure of the metal, we find that the low energy cutoff is better described than with an expression which does not contain these details.

4.6 Proposed experiments

A number of experiments which may serve to clarify various features of the present mechanism of CTRIPS phenomena are the following:

1. While cutoff experiments were performed for Pt(111), none were performed for Au(111). The difference in Shockley states in the two metals would yield differences in the cutoffs, if the present mechanism is correct. The position of the Shockley states at the Pt(111) surface is about 1.2 eV above the Fermi level [57], while those at the Au(111) surface are slightly above Fermi level. However, this difference of about 1 eV may result in a difference in the thresholds for photoemission, if the role of the surface states is nonradiative. From this viewpoint, $E_{R,th}$ for Au(111) should be about 1 eV lower than that for Pt(111). An experiment which determines the $E_{R,th}$ for Au would be clearly useful in clarifying the actual role of the surface states.

2. In only one article was the relative emission intensity of the electron and hole injection compared. More spectra which compare the relative intensities of the two emissions in Au(111) are of interest. Au(111) has allowed bulk transitions below the Fermi level, while it does not have any allowed bulk transitions above

the Fermi level up to about 3.6 eV. Thus, the hole spectra should be much more intense than the electron spectra, as is observed in the factor of fifty in the early experiments [52] with Au(111). It would be useful to have such comparisons for Pt(111), since intensities can give information as to whether a transition is allowed or indirect.

3. After the initial experiments of McIntyre and Sass [52], there have been no experiments which measure photoemission at different angles. The theoretical model presented in this chapter is fairly simple and cannot in its present form be used to explain angle resolved spectra. As mentioned, such angle resolved spectra are few and their exact peak structure is not clear. If such experiments become available, the present model can be easily adapted to include accurate coupling matrix elements and to calculate the angle resolved peak structures in light emission spectra. In the case of vacuum inverse photoemission, **k**-resolved experiments are performed and provide detailed information on the positions of band edges and surface states [51]. The contribution to the spectrum in the solution case arises, in contrast with the vacuum experiments, from a wide distribution of $\mathbf{k}_{\|}$ and k_z, reflected in the fact that in electron transfer the wave-function of the reactant can be Fourier-decomposed into many such states. Nevertheless, the increasing detail, such as that obtained by Sass and McIntyre, can elucidate the energetic positions and angular dispersion of the upper and lower states involved in the emission.

4. McIntyre and Sass [54] presented data on the difference in emission spectra of the s and p polarized light. When interpreted via a model such experiments can provide information about the optical matrix elements of the transitions and thus about the bands which contribute to the emission. An sp to d transition gives p polarized light while an sp to sp transition should emit s polarized light, provided the two bands differ in their sp content. Au(111) has few d states above the Fermi level while Pt(111) has a large d band at Fermi level. A polarization resolved spectrum at Pt(111) and Au(111) surfaces can help clarify

the role of the d states in the emission. A hole injection spectrum could also be obtained from both Au and Pt. There maybe a difference in peak position of these two spectra since the d states of the two metals are at different positions relative to the Fermi level. In some previous calculations [42] we found that d-states contribute much less, per state, than do sp-states to some electon transfer processes. It is likely that such effects occur in the CTRIPS experiments when the electron or hole is injected into d-states. The reduction in intensity might not occur in the optical matrix element $H_{k_1k_2}$ since the coupling is of a different nature from that in electron transfer H_{Dk_1}.

5. Thus far, no effects of concentration or specific adsorption of the supporting electrolyte on the spectrum appear to be available, either in CTRIPS or in electroreflectance. In principle, a decrease in concentration would make the double layer more diffuse and could lead to a smaller change in the relative position of the surface states with respect to bulk states. A change in the supporting electrolyte from one which specifically adsorbs to one which does not would also lead to a similar change. An example of such an experiment would be one using tetraalkyl ammonium ions with different alkyl chain lengths [61, 75]. If there is a significant effect on electroreflectance then there could be a significant effect on CTRIPS.

4.7 Conclusion

In the present chapter the various experimental results for charge transfer inverse photoemission spectroscopy, CTRIPS, are summarized and a theory is proposed for their treatment. This model reproduces approximately the various features of the emission spectra, including the high and low frequency cutoffs at a given E_{inj}. The question of the role of surface states is also addressed. A number of different experiments which serve to test the ideas are proposed. Since the mechanism can depend upon band structure, as discussed in Section 4.5, such experiments can also help

differentiate among possible mechanisms of photemission. The mechanism proposed in the present chapter is applicable to the band structure for Au and Pt electrodes. Ultimately with increasingly detailed experiments it can be expected that charge transfer inverse photoemission spectroscopy can be a useful technique for probing the electronic structure and behavior of metal-solution interfaces. While the once active field of CTRIPS has died out, perhaps reflecting the lack of experimental-theoretical interaction that so enriched other areas of electron transfer chemistry, we hope that the proposed experiments and tests of theoretical ideas will stimulate its revival.

Chapter 5

Conclusions

The overall theme of this thesis is the study of nonadiabatic electron transfer at metal surfaces. In Chapter 2, we developed a methodology for writing the **k**-dependent wavefunction of a semi-infinite metal using the Z-transform. We then used this method to calculate the effect of metal density of electronic states on the electron transfer rate constant, k_{ET}. We observed that the rate constant is not proportional simply to the density of states, but instead to the density of states modulated by the electronic coupling matrix elements for each of the bands. We found, consistent with electron emission results [36] and electron transfer experiments [7, 8], that the *d*-band states couple weakly to the outside environment. The coupling matrix elements significantly reduce the effect of the extra density of states of weakly coupled bands, such as the *d*-band. Thus, it is the electronic coupling modulated density of states which enters into the calculation of k_{ET}. Thereby, k_{ET} is approximately independent of ρ_{F} in two cases: adiabatic electron transfer and nonadiabatic electron transfer when the effect of any extra ρ_{F} is reduced by a weak electronic coupling.

In Chapter 3, we used the method of the Z-transform to study the effect of temperature on the nonadiabatic k_{ET}. We also compared the case of metals to that of semiconductors. The two differences between metals and nondegenerate semiconductors are: (A) The metal electrons obey the Fermi-Dirac statistics while the classical Boltzmann distribution is used for the semiconductor electrons. (B) The semiconductor-acceptor coupling, H_{kA} which contributes via eq 3.15 and eq 3.19 to k_{ET}^{max}, is approximately proportional to k_{z} in the free-electron model for the semicon-

ductor [47]. Thus, $|\overline{V}(\epsilon)|^2$ is proportional to k_z^2 and to ϵ, the transfer being from the conduction band edge. In the the metal, however, there are no significant band gaps near the Fermi energy. The distribution of the **k**'s is hardly changed when the energy, ϵ, relative to the Fermi level is changed. Thus, the coupling, $|\overline{V}(\epsilon)|^2$ is essentially independent of ϵ.

These two factors together, nevertheless, gave rise to a proportionality of the electronic factor to k_BT for k_{ET} for the exchange current in the case of the metal and for k_{ET}^{max} in the case of the maximum rate constant for the semiconductor.

In Chapter 4 we studied light emission at the metal-solution interface. The experimental results for charge transfer inverse photoemission spectroscopy, CTRIPS, were summarized and a theory is proposed for their treatment. The model reproduced approximately the various features of the emission spectra, including the high and low frequency thresholds at a given E_{inj}. We addressed the role of surface states, and proposed a mechanism for light emission, applicable to Au/Pt/Pd electrodes, which explained the cut-offs at Pt(111). We propose several different experiments which serve to test the ideas. Since the mechanism of light emission depends upon band structure, such experiments can also help differentiate among possible mechanisms of photon emission.

Bibliography

[1] R. Cannon, Electron Transfer Reactions, Butterworths, London, 1980 and references cited therein.

[2] (a) For example, for ET in biological processes there is a review article by B. E. Bowler, A. L. Raphael and H. B. Gray, *Prog. Inorg. Chem.* **38**, 259 (1990) and references cited therein. C. C. Moser, J. M. Keske, K. Warncke, R. S. Farid and P. L. Dutton, *Nature* **355**, 796 (1992); I. Bertini, H. B. Gray, S. J. Lippard and J. Valentine, Bioinorganic Chemistry University Science Books, Mill Valley, CA, 1994; (b) for organic bridges, see, for example, G. L. Closs and J. R. Miller, *Science* **240**, 440 (1988); (c) for theoretical works on the electronic coupling of long range ET, see, for example, S. Larsson and M. Braga, *Int. J. Quantum Biol. Symp.* **S20**, 65 (1993) and references cited therein; J. Logan and M. D. Newton, *J. Phys. Chem.* **92**, 3049 (1988); M. D. Newton, *Chem. Rev.* **91**, 767 (1991) and references cited therein; J. R. Reimers and N. S. Hush, *Chem. Phys.* **146**, 89 (1990); J. N. Onuchic, P. C. P. de Andrade and D. N. Beratan, *J. Chem. Phys.* **95**, 1131 (1991); P. Siddarth and R. A. Marcus, *J. Phys. Chem.* **97**, 13078 (1993), and references cited therein; (d) P. Siddarth and R. A. Marcus, *ibid* **96**, 3213 (1992); *ibid* **97**, 2400 (1993).

[3] Experimental investigations of electron transfer across self-assembled monolayers on electrode surfaces include those of J. N. Richardson, S.R. Peck, L. S. Curtin, L. M. Tender, R. H. Terrill, M. T. Carter, R. W. Murray, G. K. Rowe and S. E. Creager, *J. Phys. Chem* **99**, 766 (1995); R. J. Forster and L. R. Faulkner *J. Am. Chem. Soc.* **116**, 5444 (1994); *ibid* **116**, 9411 (1994); J. F. Smalley, S. W. Feldberg, C. E. D. Chidsey, M. R. Linford, M. D. Newton and

Y. P. Liu *J. Phys. Chem* **99**, 13141 (1995); M. S. Ravenscroft and H. O. Finklea *J. Phys. Chem* **98**, 3843 (1994); Z. Q. Feng, S. Imabayashi, T. Kakiuchi and K. Niki *J. Elec. Chem.* **394**, 149 (1995); C. E. D. Chidsey *Science* **251**, 919 (1991); *ibid.* **252**, 631 (1991).

[4] T. Iwasita, W. Schmickler, J. W. Schultze, *Ber. Bensunges. Phys. Chem.* **89**, 138 (1985).

[5] T. T.-T. Li, H. Y. Liu, M. Weaver, *J. A. C. S.* **106**, 1233 (1984).

[6] A. Capon, R. Parsons, *J. Electroanal. Chem. Inter. Electrochem. 46*, 215 (1973).

[7] H. O. Finklea, personal communication. These experiments were performed with the same system that was used in this chapter and gave a ratio ($k_{\mathrm{Pt}}/k_{\mathrm{Au}}$) of ~ 1.

[8] R. J. Forster, P. Loughman, D. P. O'Hanlon, manuscript in preparation. To be submitted to *J. Phys. Chem. B*. These experiments have been performed with $(\mathrm{Os(bpy)_2p3pCl})^+$ monolayers and gave a ratio ($k_{\mathrm{Pt}}/k_{\mathrm{Au}}$) of 2.3.

[9] C. E. D. Chidsey, *Science* **251**, 919 (1991).

[10] H. O. Finklea, in: A. J. Bard, I. Rubenstein (Eds.), Electroanalytical Chemistry, vol. 19, Marcel-Dekker Inc, New York, 1996, 109 and references cited therein.

[11] D. A. Papaconstantopoulous, Handbook of Band Structure of Elemental Solids, Plenum Press, New York, 1986.

[12] R. Hoffmann, *J. Chem. Phys.* **39**, 1397 (1963). We use the following program: M. H. Whangbo, *Extended Hückel Molecular Crystal Properties Package* (QCPE Program No. 571).

[13] (a) C.-P. Hsu, R. A. Marcus, *J. Chem. Phys.* **106 (2)**, 584 (1997).
(b) C.-P. Hsu, *J. Electroanal. Chem.* **438**, 27 (1997).

[14] R. A. Marcus, *J. Chem. Phys.* **98 (7)**, 5604 (1993) and references cited therein.

[15] A. A. Stuchebrukhov, R. A. Marcus, *J. Phys. Chem.* **99**, 7581 (1995).

[16] P. Siddarth, R. A. Marcus, *J. Phys. Chem.* **97**, 6111 (1993).

[17] R. A. Marcus, *J. Chem. Phys.* **43**, 679 (1965), and references cited therein.

[18] This expression for the rate constant includes the assumption that the solvent's dielectric polarization is not "sluggish."

[19] The density of states at a given energy ϵ is

$$\rho = \int d^3k \; \delta(\epsilon(\mathbf{k}) - \epsilon).$$

This density can be calculated using the above equation in conjunction with eq 2.25. A grid is set up in **k**-space to choose **k**-vectors; eq 2.25 is then solved to obtain eigen-energies and a binning technique is used to obtain the density of states from the eigen-energies using the above expression for ρ.

In the Z-transform formulation a reverse procedure is used, in which for any given energy ϵ, the $\mathbf{k}_{\|}$ values are used to find z, by solving eq 2.33 in Section 2.4. (The $\mathbf{k}_{\|}$ determine the $\mathbf{B}^{\dagger}$, $\mathbf{A}$ and $\mathbf{B}$ that appear in eq 2.33.)

[20] A. V. Oppenheim, A. V., A. S. Wilsky, I. T. Young, Signals and Systems, Prentice-Hall Inc., New Jersey, 1983.

[21] A capital letter used here for a vector indicates a vector which can take on discrete values, i.e., a vector which points from one atom to another atom, both in the crystal.

[22] J. C. Slater, G. F. Koster, *Phys. Rev.* **94 (6)**, 1498 (1954).

[23] If there is three dimensional translational symmetry (in bulk), we speak of a 3-D wavevector. In this derivation we use $\mathbf{k}_{\|}$ to denote the part of the wavevector parallel to the plane, and k_m to denote the part of the wavevector along the third axis of the unit cell, frequently perpendicular to the plane, if $\mid z \mid = 1$.

In general, if a surface is present, it mixes k_m's and k_m is not a good quantum number.

[24] D. H. Lee, J. D. Joannopoulos, *Phys. Rev. B* **23**, 4988 (1981).

[25] CRC Handbook of Chemistry and Physics, D. R. Lide (Ed.), 74rd ed., CRC Press, 1993-94.

[26] H. Ou-Yang, B. Kallebring, R. A. Marcus, *J. Chem. Phys.* **98**, 7145 (1993).

[27] C. Kittel, Introduction to Solid State Physics, 7th ed., John Wiley and Sons, New York, 1995.

[28] Y. K. Shin, D. J. Szalda, B. S. Brunschwig, C. Creutz, N. Sutin, *Inorg. Chem.* **36**, 3190 (1997).

[29] These 60 vectors are chosen randomly. Because of the surface there is no symmetry in the direction perpendicular to the surface. The symmetry in the remaining two directions cannot be exploited either because of the presence of the monolayer. A simpler calculation based on eq 2.7 was performed with 600 vectors. We find that the ratio $k_{\mathrm{Pt}}/k_{\mathrm{Au}}$ changes from about 1.74 to 1.80 on going from 60 to 600 wave vectors. This seems to be a small enough variation that we use 60 vectors to perform the rest of our calculations.

[30] Using the work functions of the metals [25] (5.7 eV for Pt and 5.31 eV for Au) and the formal potential of $\mathrm{pyRu(NH_3)_5^{2+}/pyRu(NH_3)_5^{3+}}$ (which is -0.08 eV above SCE [7]) we find that the difference in energy of the two states is

$$\Delta E = E_{metal} - \Psi_B - \Delta\epsilon_i,$$

where E_{metal} is -4.97 eV for Au and -5.16 eV for Pt. Ψ_B is the ionization potential of the bridge and $\Delta\epsilon_i$ is the difference in energy of the electronic state of the electron in the bridge and of the HOMO of the bridge.

[31] R. A. Marcus, N. Sutin, *Biochim. et Biophys. Acta* **811**, 265 (1985).

[32] H. O. Finklea, M. S. Ravenscroft, *Israel J. Chem.* **37**, 179 (1997).

[33] See for example: D. G. Evans, *Inorg. Chem.* **25**, 4602 (1986) and R. G. Woolley, *Inorg. Chem.* **27**, 430 (1988).

[34] See for example: A. A. Stuchebrukhov, R. A. Marcus, *J. Chem. Phys.* **98**, 6044 (1993) and references therein.

[35] A. Kiejna, A. and K. F. Wojciechowski, Metal Surface Electron Physics, Pergamon, 1996.

[36] Gadzuk, J. W. *Phys. Rev.* **182**, 416 (1969).

[37] J. W. Gadzuk, W. E. Plummer, *Rev. Mod. Phy.* **45**, 487 (1973) and references cited therein.

[38] C. E. D. Chidsey *Science* **251**, 919 (1991); *ibid.* **252**, 631 (1991); C. Miller, M. Grätzel, *J. Phys. Chem.* **95**, 5225 (1991); H. O. Finklea, D. D. Hanshew, *J. Am. Chem. Soc.* **114**, 3173 (1992); A. M. Becka, C. J. Miller, *J. Phys. Chem.* **96**, 2657 (1992); H. O. Finklea, M. S. Ravenscroft, D. A. Snider, *Langmuir* **9**, 223 (1993); M. S. Ravenscroft, H. O. Finklea, *J. Phys. Chem.* **98**, 3843 (1994); L. M. Tender, M. T. Carter, R. W. Murray, *Anal. Chem.* **66**, 3173 (1994); K. Weber, S. E. Creager, *Anal. Chem.* **66**, 3164 (1994); G. K. Rowe, M. T. Carter, J. N. Richardson, R. W. Murray, *Langmuir* **11**,1797 (1995); K. Weber, L. Hockett, S. Creager, *J. Phys. Chem. B* **101**, 8286 (1997); H. O. Finklea, M. S. Ravenscroft, *Israel J. Chem.* **37**, 179 (1997); S. Sek, A. Misicka, R. Bilewicz, *J. Phys. Chem. B* **104**, 5399 (2000).

[39] J. F. Smalley, S. W. Feldberg, C. E. D. Chidsey, M. R. Linford, M. D. Newton, Y.-P. Liu, *J. Phys. Chem.* **99**, 13141 (1995);

[40] J. N. Richardson, G. K. Rowe, M. T. Carter, L. M. Tender, L. S. Curtin, S. R. Peck, R. W. Murray, *Electrochim. Acta* **40**, 1331 (1995); M. T. Carter, G. K. Rowe, J. N. Richardson, L. M. Tender, R. H. Terrill, R. W. Murray, *J. Am.*

Chem. Soc. **117**, 2896 (1995); J. N. Richardson, S. R. Peck, L. S. Curtin, L. M. Tender, R. H. Terrill, M. T. Carter, R. W. Murray, G. K. Rowe, S. E. Creager, *J. Phys. Chem.* **99**, 766 (1995); K. S. Weber, S. E. Creager, *J. Electroanal. Chem.* **458**, 17 (1998).

[41] I. S. Gradshteyn, I. M. Ryzhik, Tables of Integrals, Series and Products, Academic Press, New York, 349, e.g., $\int_{-\infty}^{\infty} g(\epsilon)d\epsilon = \pi k_B T$, $\int_{-\infty}^{\infty}(\epsilon/2)^4 g(\epsilon)d\epsilon = (\pi k_B T)^5(5/16)$, $\int_{-\infty}^{\infty}(\epsilon/2)^6 g(\epsilon)d\epsilon = (\pi k_B T)^7(61/64)$.

[42] S. Gosavi, R. A. Marcus, *J. Phys. Chem. B***104**, 2067 (2000). In this reference and the present chapter the surface of the metal is a (111) face. For some simpler surfaces with more symmetry elements, the Z-transform method that we use is not necessary and the wavefunctions can be described in these cases by a simple sine-like function. We use extended Hückel (EH) to calculate the bridge coupling matrix elements in both the above article and the present chapter. The EH method gives more accurate results for relative matrix elements and rates than it does for absolute values.

[43] Y. Q. Gao, Y. Georgievskii, R. A. Marcus, *J. Chem. Phys.***112**, 3358 (2000). The $V_{\mathbf{k}}$ in this article is denoted in the present chapter by H_{kA}. Since the form of the electronic matrix element is the same for both semiconductors and metals eqs 3.4, 3.15, and 3.16 remain valid for both types of electrodes.

[44] N. S. Lewis, *Z. Phys. Chem.* **212**, (1999) and references cited therein.

[45] R. A. Marcus, *J. Chem. Soc. Faraday Trans.92*, 3905 (1996).

[46] For a particular fit function we find a value of $b = -10.84$ and $d = 203.47$ which gives an average correction of 0.96 for a $k_B T$ range of $\sim$ 0.01 eV to 0.027 eV, i.e., $120K \leq T \leq 325K$. Because of the peak of the Pt curve in Fig. 3.2 at Fermi energy, the slopes of the Pt plots in Fig. 3.3 are sensitive to the fitted polynomial used.

[47] Y. Q. Gao, R. A. Marcus, *J. Chem. Phys.* **113**, 6351 (2000). If in other cases, H_{kA} were proportional to a linear combination of $k_{\rm x}$, $k_{\rm y}$ and $k_{\rm z}$, then $|H_{kA}|^2$ averaged near the conduction band edge would still be proportional to ϵ. In general, Ψ_k and thus the matrix element is proportional to $\sin(k_{\rm z})$, which becomes $k_{\rm z}$ only at a band edge (small $k_{\rm z}$). Like $k_{\rm z}$, the distribution of $\sin(k_{\rm z})$'s is hardly changed when ϵ is changed in the case of a metal since $\Delta >> \epsilon$.

[48] K. W. Böer, Survey of Semiconductor Physics, VNR, New York, 1990, 215. In the case of indirect bandgap semiconductors the $k_{\rm x}$, $k_{\rm y}$ and $k_{\rm z}$'s are replaced by $k_{\rm x} - k_0$, $k_{\rm y} - k_0$ and $k_{\rm z} - k_0$ throughout and the same conclusion applies.

[49] (a) R. Schneider, V. Dose, Unoccupied Electronic States, J. C. Fuggle, J. E. Inglesfield, (Eds.) Springer-Verlag, 1991, (b) S. Hufner, Photoelectron Spectroscopy, Springer-Verlag, 1996.

[50] (a) J. B. Pendry, *Phys. Rev. Lett.* **45**, 16 (1980). (b) J. B. Pendry, *J. Phys. C* **14**, 1381i (1981). (c) G. Borstel, G. Thorner, *Surf. Sci. Reps.* **8**, 1 (1987) and references therein.

[51] V. Dose, *Surf. Sci. Reps.* **5**, 337 (1985) and references therein.

[52] R. McIntyre, J. K. Sass, *P. R. L.* **56**, 651 (1986). (a) Fig. 2 and Fig. 3a (b) Fig. 3b (c) Fig. 2: 0.9 V spectrum.

[53] S. H. Liu, C. Hinnen, C. Nguyen Van Huong, N. R. De Tacconi, K. M. Ho, *J. Electroanal. Chem.* **176**, 325 (1984).

[54] R. McIntyre, D. K. Roe, J. K. Sass, H. Gerischer, Electrochemical Surface Science, M. P. Soriaga, (Ed.) American Chemical Society: Washington DC, 1988, p. 233. (a) Fig. 5 (b) Fig. 3.

[55] J. Ouyang, A. J. Bard, *J. Phys. Chem.* **91**, 4058 (1987). (a) Fig. 7c

[56] J. Ouyang, A. J. Bard, *J. Phys. Chem.* **92**, 5201 (1988). (a) Fig. 6

[57] C. G. Larsson, P. O. and Nilsson, *Phys. Lett. A* **85A**, 393 (1981).

[58] K. Uosaki, K. Murakoshi, H. Kita, *J. Phys. Chem.* **95**, 779 (1991). (a) Fig. 6

[59] K. Murakoshi, K. Uosaki, *J. Phys. Chem.* **96**, 4593 (1992). (a) Fig. 10 (b) Fig. 4 (c) Fig. 2: 0.2 V spectrum (d) Fig. 4b (e) Fig. 8.

[60] K. Murakoshi, K. Uosaki, *Phys. Rev. B* **47**, 2278 (1993). (a) Fig. 5

[61] A. J. Bard, L. R.and Faulkner, Electrochemical Methods, John Wiley and Sons, 1980.

[62] K. Murakoshi, K. Uosaki, *J. Electroanal. Chem.* **308**, 351 (1991).

[63] K. Murakoshi, K. Uosaki, *J. Vac. Sci. Tech. A* **10**, 2981 (1992).

[64] E. Merzbacher, Quantum Mechanics, John Wiley and Sons, 1961.

[65] The factor T_{ind} is obtained from the difference in light emission intensity between hole and electron transitions at 2.9 eV above and below the Fermi level respectively. The electron transitions are mainly indirect transitions due to a band gap present above the Fermi level in the $\Gamma - L$ direction of the Au(111) surface. The hole transitions on the other hand are inferred to be direct transitions [52] between a low lying d-band and an sp-band at the Fermi level. The density of d-states is higher than the densities of the sp-bands present above the Fermi level and, this fact should enter into a more accurate calculation. In an earlier calculation [42] we found that the d-bands couple weakly and thus the contribution from any extra density of states does not make a large difference to the electron transfer rate constant. We use this fact in the present calculation and assume that the effective density of states is approximately constant as a function of energy.

[66] R. A. Marcus, *Electrochim. Acta* **13**, 995 (1968).

[67] Photoemission in Solids I and II, M. Cardona, L. Ley (Eds.), Springer-Verlag, 1978.

[68] (a)N. J. Shevchik, *Phys. Rev. B* **16**, 6428 (1977), (b)V. M. Tapilin, *Surf. Sci.* **383**, 226 (1997).

[69] D. M. Kolb, *Angew. Chem. Int. Ed.* **40**, 1162 (2001) and references cited therein.

[70] W. Schmickler, *Chem. Rev.* **96**, 3177 (1996) and references cited therein.

[71] D. P. Woodruff, W. A. Royer, N. V. Smith, *Phys. Rev. B* **34**, 764 (1986).

[72] U. W. Hamm, D. Kramer, R. S. Zhai, D. M. Kolb, *J. Electroanal. Chem.* **414**, 85 (1996).

[73] D. M. Kolb, C. Franke, *Appl. Phys. Lett. A* **49**, 379 (1989).

[74] A. Kokalj, M. Causa, *J. Phys. Cond. Matter* **11**, 7463 (1999).

[75] A. P. Abbott, J. C. Harper, G. Stimsom, *J. Electroanal. Chem.* **520**, 6 (2002) and references therein.